

Balanced Input from the tRNA Prenyltransferase MiaA Controls the Stress Resistance and Virulence Potential of Extraintestinal Pathogenic *Escherichia coli*

Matthew G. Blango^{*†◇}, Brittany A. Fleming^{*†}, William M. Kincannon[‡], Alex Tran^{*}, Adam J. Lewis^{*}, Colin W. Russell^{*}, Qin Zhou^{*}, Lisa M. Baird[§], John R. Brannon[¶], Connor J. Beebout[¶], Vahe Bandarian[‡], Maria Hadjifraniskou[¶], Michael T. Howard[§], and Matthew A. Mulvey^{*#}

^{*}Division of Microbiology and Immunology, Pathology Department, University of Utah School of Medicine, Salt Lake City, Utah.

[‡]Department of Chemistry, University of Utah, Salt Lake City, Utah.

[§]Department of Human Genetics, University of Utah, Salt Lake City, Utah.

[¶]Department of Pathology, Microbiology, and Immunology, Vanderbilt University Medical Center, Nashville, Tennessee.

[◇]Current address: Junior Research Group RNA Biology of Fungal Infections, Leibniz Institute for Natural Product Research and Infection Biology (Leibniz-HKI), Jena, Germany.

[†]These authors contributed equally to the work. Listed alphabetically.

[#]Corresponding author:

Phone: 801-581-5967

E-mail: mulvey@path.utah.edu

1 **ABSTRACT**

2 An ability to adapt to rapidly changing and often hostile environments is key to the success
3 of many bacterial pathogens. In *Escherichia coli*, the highly conserved enzymes MiaA
4 and MiaB mediate the sequential prenylation and methylthiolation of adenosine-37 within
5 tRNAs that decode UNN codons. Here, we show that MiaA, but not MiaB, is critical to the
6 fitness and virulence of extraintestinal pathogenic *E. coli* (ExPEC), a major cause of
7 urinary tract and bloodstream infections. Deletion of *miaA* has pleiotropic effects,
8 rendering ExPEC especially sensitive to stressors like nitrogen and oxygen radicals and
9 osmotic shock. We find that stress can stimulate striking changes in *miaA* expression,
10 which in turn can increase translational frameshifting and markedly alter the bacterial
11 proteome. Cumulatively, these data indicate that ExPEC, and likely other organisms, can
12 vary MiaA levels as a means to fine-tune translation and the spectrum of expressed
13 proteins in response to changing environmental challenges.

14

15

16

17

18

19 INTRODUCTION

20 The translation of mRNA into protein by ribosomes and aminoacyl-transfer RNA
21 (tRNA) complexes is an energy-intensive process that is subject to multiple levels of
22 complicated regulation. For example, tRNAs can be covalently modified by more than 100
23 different moieties that can influence the charging of tRNAs with amino acids, tRNA
24 stability, codon usage, and reading frame maintenance [1-4]. In *Escherichia coli* and other
25 bacteria, the hypomodification of tRNAs can result in decreased growth rates, altered
26 metabolic requirements, and reduced stress resistance [5-8]. Loss of tRNA modifications
27 can also impact the fitness and virulence potential of many important bacterial pathogens,
28 including *Streptomyces pyogenes*, *Pseudomonas spp.*, *Shigella flexneri*, *Agrobacterium*
29 *tumefaciens*, *Mycobacterium tuberculosis*, *Aeromonas hydrophila*, *Streptococcus spp.*,
30 and *Salmonella enterica* serotype Typhimurium [6, 9-21]. Together, these findings
31 suggest that tRNA modification serves as a regulatory nexus that can control a wide array
32 of bacterial activities.

33 One of the most commonly modified tRNA residues in bacteria is adenosine-37 (A-
34 37), which lies adjacent to the anticodon loop [8, 22]. In its final form in *E. coli*, A-37 of
35 UNN-recognizing tRNA molecules is oftentimes prenylated and methylthiolated [23]. The
36 *miaA* gene of *E. coli* encodes a tRNA prenyltransferase that catalyzes the addition of a
37 prenyl group onto the N^6 -nitrogen of A-37 to create i^6 A-37 tRNA [24, 25] (**Fig. 1A**). The
38 modified i^6 A-37 residue is subsequently methylthiolated by the radical-S-
39 adenosylmethionine enzyme MiaB to create ms^2i^6 A-37 [26]. The bulky and hydrophobic
40 ms^2i^6 A-37 modification enhances tRNA interactions with UNN target codons, promoting
41 reading frame maintenance and translational fidelity [5, 8, 27]. Mutations in the *miaA* locus

42 result in an unmodified A-37 residue, as prenylation is required for methylthiolation by
43 MiaB. In K-12 laboratory-adapted *E. coli* strains, mutations in *miaA* impair attenuation of
44 the tryptophan and phenylalanine operons [28, 29] and diminish translation of the
45 stationary phase sigma factor RpoS and the small RNA chaperone Hfq [7, 30, 31].
46 Additionally, mutants lacking *miaA* are unable to effectively resolve aberrant DNA-protein
47 crosslinks [32] and have somewhat elevated spontaneous mutation frequencies [33-35].
48 The ms²ⁱ⁶A-37 modification is highly conserved in both prokaryotes and eukaryotes,
49 though the specific enzymes that mediate this modification have diverged within
50 evolutionarily distant organisms [8]. However, in prokaryotes, MiaA and MiaB
51 homologues are relatively well conserved, and the enzymes appear to function similarly
52 in all tested bacterial species [36, 37].

53 Given that the ms²ⁱ⁶A-37 modification is a well-defined regulator of many tRNA
54 functions in lab-adapted K-12 *E. coli* strains, we sought to understand how this
55 modification is co-opted in a pathogenic *E. coli* background. *E. coli* pathotypes display
56 extensive genetic diversity and are usually more resilient under stress than their lab-
57 adapted counterparts [38]. Extraintestinal Pathogenic *E. coli* (ExPEC) typically reside in
58 the lower intestinal tract of mammals, where they are rarely associated with pathology
59 [39]. However, when they spread outside the gut to other host sites ExPEC can cause a
60 number of serious diseases, including urinary tract and bloodstream infections [38, 40].
61 Bacterial pathogens like ExPEC must be able to rapidly respond to a diverse array of
62 stressors encountered within changing host environments. These include nutrient
63 deprivation, redox stress in the form of oxygen and nitrogen radicals, extremes in pH,

64 envelope damage, changing osmotic pressures, and a wide assortment of host immune
65 effector cells and antimicrobial compounds [41-45].

66 Shifts in the prevalence of specific tRNA modifications, such as A-37 prenylation
67 mediated by MiaA, are proposed to help optimize bacterial responses to stress by
68 affecting translational fidelity and selective protein expression [14, 33, 46]. In other words,
69 changing levels of tRNA modifications may control the codon-biased translation of select
70 transcripts, providing a post-transcriptional programmable mechanism that distressed
71 cells can use to facilitate beneficial changes in their proteomes. Here we provide evidence
72 in support of this hypothesis, showing that ExPEC can modulate MiaA levels in response
73 to stress, and that varying levels of this enzyme can increase translational frameshifting
74 and markedly alter the spectrum of expressed proteins. Furthermore, our data reveal that
75 MiaA, but not MiaB, is critical to the fitness and virulence of ExPEC in both *in vitro* assays
76 and in mouse models of infection and intestinal colonization.

77

78 **RESULTS**

79 ***MiaA promotes ExPEC fitness and virulence in vivo***

80 To assess the importance of MiaA and MiaB for ExPEC within varied host
81 environments, we employed well-established mouse models of gut colonization, urinary
82 tract infection (UTI), and bloodstream infection [47]. For these and subsequent
83 experiments, *miaA* and *miaB* were independently deleted from the ExPEC reference
84 strain UTI89 to generate the isogenic knockout mutants UTI89 Δ *miaA* and UTI89 Δ *miaB*
85 [48, 49].

86 *Gut colonization.* The mammalian gastrointestinal (GI) tract serves as a major
87 reservoir for ExPEC that can seed extraintestinal infections [50-54]. Roles for MiaA and
88 MiaB in ExPEC colonization of the GI tract were probed using competitive assays in which
89 $\sim 10^9$ colony forming units (CFU) of a 1:1 mixture of UTI89 and either UTI89 $\Delta miaA$ or
90 UTI89 $\Delta miaB$ were introduced into adult specific-pathogen-free (SPF) BALB/c mice via
91 intragastric gavage [55-57]. In this model system, the levels of ExPEC recovered from the
92 feces reflect ExPEC titers within the large intestines [55]. For these assays, UTI89 and
93 the *miaA* and *miaB* knockout mutants were engineered to express either kanamycin
94 (Kan^R) or chloramphenicol (Cam^R) resistance cassettes so that the strains could be
95 readily identified by plating fecal homogenates on selective media. Feces were collected
96 at the indicated time points and the numbers of viable bacteria were enumerated to
97 determine competitive indices (CI). UTI89 $\Delta miaA$ was significantly outcompeted by wild-
98 type UTI89 as early as day 3 post-inoculation (**Fig. 1B**). By day 10, there was about a
99 25,000-fold reduction in the relative levels of UTI89 $\Delta miaA$ recovered from the feces,
100 correlating with a median CI of -4.39. At this time point, UTI89 $\Delta miaA$ titers in the majority
101 of mice were below the limit of detection. In contrast, there were no notable differences
102 in titers between UTI89 $\Delta miaB$ and UTI89 in the feces at any time point (**Fig. 1C**). These
103 results indicate that the loss of MiaA, but not MiaB, greatly impairs the fitness of UTI89
104 within the gut

105 *UTI.* During the course of a UTI, ExPEC is able to bind and invade the host
106 epithelial cells that comprise the bladder mucosa [58]. Once internalized into bladder
107 cells, ExPEC can traffic into late endosome-like compartments where it may form
108 quiescent reservoir populations that promote long-term bacterial persistence.

109 Alternatively, ExPEC can enter the host cytosol and rapidly multiply, forming large
110 intracellular bacterial communities that eventually rupture the epithelial cell. In cell culture-
111 based assays using a bladder epithelial cell line, we found that UTI89 $\Delta miaA$ and
112 UTI89 $\Delta miaB$ are able to bind, invade, and survive intracellularly in overnight assays much
113 like wild-type UTI89 (**Supplemental Fig. S1**).

114 To investigate MiaA and MiaB requirements during UTI, 10^7 CFU of wild-type
115 UTI89, UTI89 $\Delta miaA$, and UTI89 $\Delta miaB$ were independently inoculated via transurethral
116 catheterization into adult female CBA/J mice and bacterial titers in the bladders were
117 determined after 3 days. In this analysis, UTI89 $\Delta miaB$ showed no statistically significant
118 defect relative to the parent strain; whereas the $\Delta miaA$ strain was clearly attenuated (**Fig.**
119 **1D**). Deficiencies in bladder colonization by UTI89 $\Delta miaA$ were apparent by 6 h post-
120 inoculation (**Supplemental Fig. S2A**), and were still significant after 9 days
121 (**Supplemental Fig. S2B**). The differences observed between wild-type UTI89 and
122 UTI89 $\Delta miaA$ at 3 days post-inoculation of CBA/J mice were also manifest in C3H/HeJ
123 mice (**Supplemental Fig. S2C**). Due to defects in Toll-like receptor 4 (TLR4) signaling
124 and other innate defenses, C3H/HeJ mice have attenuated inflammatory responses and
125 increased susceptibility to UTI [59-62]. Our results indicate that the decreased capacity
126 of UTI89 $\Delta miaA$ to colonize the bladder is not attributable to an inability of the *miaA*
127 knockout to handle TLR4-dependent innate host defenses. Collectively, these results
128 indicate that MiaA is required for maximal fitness in mouse UTI models, while MiaB is less
129 critical.

130 *Bloodstream infection.* ExPEC is a leading cause of bloodstream infections, which
131 too often trigger discordant systemic inflammatory responses that can result in a life-

132 threatening condition known as sepsis [63]. To examine the contributions of MiaA and
133 MiaB to ExPEC virulence and fitness in a model of sepsis, adult C57Bl/6 mice were
134 inoculated via intraperitoneal (i.p.) injections with $\sim 10^7$ CFU of wild-type UTI89,
135 UTI89 $\Delta miaA$, or UTI89 $\Delta miaB$. Following i.p. injection, the bacteria enter the bloodstream
136 and disseminate [56, 64, 65]. In our experiments, only 15% (2/13) of the mice infected
137 with wild-type UTI89, and 0% (0/13) of the mice injected with UTI89 $\Delta miaB$, were viable
138 after 48 hours (**Fig. 1E**). In sharp contrast, 84% (11/13) of the mice infected with
139 UTI89 $\Delta miaA$ survived. At six hours post-injection, significantly lower numbers of bacteria
140 were recovered from the spleens and kidneys of UTI89 $\Delta miaA$ -infected mice, relative to
141 mice infected with wild-type UTI89 or UTI89 $\Delta miaB$ (**Supplemental Fig. S3A and B**).
142 While not significant, titers in the liver also trended lower in UTI89 $\Delta miaA$ -infected mice
143 (**Supplemental Fig. S3C**). Combined, these data demonstrate that MiaA is important for
144 the virulence of ExPEC and its survival during systemic infections, while MiaB appears
145 dispensable.

146

147 ***MiaA enhances ExPEC growth and stress resistance***

148 Earlier studies showed that K-12 *E. coli* and *Salmonella* mutants lacking *miaA* are
149 moderately impaired in nutrient-rich broth, but less so in nutrient-limited media [27, 35,
150 66]. Using *in vitro* growth assays, we found that UTI89 $\Delta miaA$ grew normally in modified
151 M9 minimal media, but failed to reach densities as high as the wild-type strain in more
152 complex, nutrient-rich lysogeny broth (LB) (**Fig. 2A and B**). In contrast, the *miaB* knockout
153 exhibited no overt growth defects in either type of media. These data suggest that
154 UTI89 $\Delta miaA$ has reduced metabolic flexibility relative to wild-type UTI89 and the *miaB*

155 mutant. This may contribute to the decreased fitness of UTI89 Δ *miaA* in our mouse
156 models, where the bacteria likely encounter marked shifts in nutrient availability.
157 However, within different host environments ExPEC will face a wide variety of additional
158 challenges that might be countered by MiaA-dependent processes. We investigated this
159 possibility by examining the effects of MiaA and MiaB on ExPEC resistance to nitrosative,
160 oxidative, and osmotic stress.

161 *Oxidative and nitrosative stress.* During the course of an infection, both host and
162 bacterial cells can produce reactive oxygen and nitrogen radicals that can damage lipids,
163 proteins, and nucleic acids [67, 68]. The contributions of MiaA and MiaB to nitrosative
164 and oxidative stress resistance were assessed using acidified sodium nitrite (ASN) and
165 methyl viologen (MV), respectively. When added to low pH morpholineethanesulfonic acid
166 (MES)-buffered LB (MES-LB; pH 5.0), sodium nitrite dismutates to form nitrous acid which
167 in turn generates NO and other harmful reactive nitrogen species [69]. In un-
168 supplemented MES-LB, UTI89 Δ *miaA* reached a lower maximal density than wild-type
169 UTI89 (**Fig. 2C**), similar to results obtained using standard LB (**Fig. 2B**). The addition 1
170 mM ASN delayed entry of UTI89 Δ *miaA* into exponential growth phase by close to 4 hours
171 (**Fig. 2D**), while 2 mM ASN delayed growth by more than 15 hours relative to wild-type
172 UTI89 (**Fig. 2E**). The addition of 1 mM MV, which produces superoxide radicals [70], had
173 even stronger inhibitory effects on growth of UTI89 Δ *miaA* (**Fig. 2F**). In contrast,
174 UTI89 Δ *miaB* grew much like the wild-type strain in the presence of ASN or MV (**Fig. 2D-**
175 **F**). Complementation with pMiaA_{nat}, a low copy plasmid that encodes MiaA under control
176 of its native promoter, restored growth of UTI89 Δ *miaA* to near wild-type levels in both 2
177 mM ASN (**Fig. 2G**) and in 1 mM MV (**Fig. 2H**).

178 *Osmotic stress.* During a UTI, osmotic pressure within the bladder can shift from
179 50 to >1,400 mOsm/kg due to varying concentrations of solutes like sodium and urea [71,
180 72]. By comparison, the normal osmolarity of blood ranges from about 275 to 295
181 mOsm/kg. To test the sensitivities of wild-type UTI89 and the knockout strains to
182 hypoosmotic stress, we diluted the bacteria from early stationary phase cultures into
183 ddH₂O, and then quantified the number of viable bacteria every 30 minutes over the
184 course of 2 hours. Titers of UTI89Δ*miaA* carrying the empty vector pACYC184 were
185 greatly reduced following exposure to hypoosmotic stress, whereas the levels of
186 UTI89/pACYC184 and UTI89Δ*miaB*/pACYC184 remained mostly unchanged (**Fig. 3A**).
187 Survival of UTI89Δ*miaA* was restored by complementation with pMiaA_{nat}. To ensure that
188 reduced survival of UTI89Δ*miaA* was attributable to hypoosmotic stress and not
189 starvation, cells were resuspended in ddH₂O containing 0.1% glucose, which is
190 comparable to the glucose levels within our M9 medium. Viable bacteria measured after
191 120 minutes indicated that the death of UTI89Δ*miaA* was not due to nutrient deprivation
192 (**Fig. 3B**). We also observed that UTI89Δ*miaA* grew poorly in hyperosmotic conditions,
193 created by addition of 5% NaCl to standard LB (**Fig. 3C**). As in other assays, UTI89Δ*miaB*
194 behaved more like the wild-type strain. Growth of UTI89Δ*miaA* was restored to wild-type
195 levels by complementation with pMiaA_{nat} (**Fig. 3D**). These results indicate that the *miaA*
196 knockout has decreased resistance to both hypo- and hyperosmotic stresses.

197

198 ***Hyperosmotic stress attenuates MiaA translation***

199 We next examined how MiaA levels in UTI89 change in response to environmental
200 cues, focusing on hyperosmotic stress. For these assays, we employed a low-copy

201 number plasmid (pMiaA-Flag_{nat}) that encodes C-terminal FLAG-tagged MiaA under
202 control of the native *miaA* promoter. Mid-logarithmic phase cultures of UTI89/pMiaA-
203 Flag_{nat} were resuspended in LB ± 5% NaCl and levels of MiaA-Flag were then assessed
204 by western blot at 30-minute intervals over the course of 1.5 hours (**Fig. 4A**). Interestingly,
205 MiaA levels in UTI89 exposed to high salt broth were decreased at all time points in
206 comparison with bacteria grown in standard LB. We observed a similar phenomenon if
207 overnight cultures of UTI89/pMiaA-Flag_{nat} in standard LB were back-diluted into high salt
208 broth and then grown to mid-logarithmic phase (OD₆₀₀≈0.5, **Fig. 4B**). Of note, in these
209 assays we observed no loss of the pMiaA-Flag_{nat} construct. In addition, *miaA* transcripts
210 were often elevated following exposure of UTI89 to high salt (**Fig. 4C**), suggesting that
211 the downregulation of MiaA protein levels in response to this osmotic stress occurs via a
212 post-transcriptional mechanism. The transcription of *miaB* was notably reduced under the
213 same conditions (**Fig. 4D**).

214 To determine if lower amounts of the MiaA protein detected in high salt broth
215 culture affected i⁶A or ms²i⁶A levels, we employed liquid chromatography-coupled mass
216 spectrometry (LC-MS). Normalized amounts of the i⁶A modification in wild-type UT89
217 grown to mid-logarithmic phase in LB were similar to those measured in UTI89 grown in
218 high salt broth (**Fig. 4E**). However, hyperosmotic stress caused a marked reduction in
219 relative ms²i⁶A levels (**Fig. 4F**), possibly due to reduced transcription of *miaB* (**Fig. 4D**).
220 i⁶A and ms²i⁶A were undetectable in UTI89Δ*miaA*, regardless of high salt exposure,
221 confirming that MiaA is required for both modifications (**Fig. 4E-F**). In contrast, deletion
222 of *miaB* prevented formation of ms²i⁶A, but led to greatly elevated levels of i⁶A
223 (**Supplemental Fig. S4**). Cumulatively, these data indicate that in response to

224 hyperosmotic stress UTI89 can post-transcriptionally downregulate MiaA, coordinate with
225 reduction of both *miaB* messages and ms²i⁶A levels.

226

227 ***Overexpression of MiaA is detrimental under stressful conditions.***

228 Since it was unexpected that high salt stress would lead to a decrease in the levels
229 of MiaA and the ms²i⁶A modification, we set out to determine if overexpression of MiaA
230 would affect bacterial growth during environmental stress. To overexpress MiaA, we
231 utilized a plasmid (pRR48) with *miaA* under control of an IPTG-inducible *Ptac* promoter
232 in wild-type UTI89. By LC-MS, relative intensities of i⁶A were significantly higher in
233 UTI89/pMiaA_{*Ptac*} induced with 1 mM IPTG and grown to mid-logarithmic phase in LB
234 compared to UTI89 carrying the empty vector pRR48, whereas the relative intensities of
235 ms²i⁶A were only modestly elevated (**Fig. 5A**).

236 Next, overnight cultures of UTI89/pMiaA_{*Ptac*} were back-diluted into LB, LB + 1 mM
237 MV, LB + 5% NaCl, MES-LB, or MES-LB + 1 mM ASN, and grown in the presence of
238 increasing IPTG concentrations (**Fig. 5B-F**). Lower levels of MiaA protein induction
239 caused no overt defects and the bacteria grew much like UTI89/pRR48. However, higher
240 levels of IPTG-induced MiaA expression hindered growth of UTI89/pMiaA_{*Ptac*} in the
241 presence of 1 mM MV, 5% NaCl, MES-LB, and 1 mM ASN. In contrast, over expression
242 of MiaB did not affect bacteria growth in these *in vitro* assays (**Supplemental Fig. S5**).
243 These findings indicate that too much MiaA can be detrimental to bacterial fitness, similar
244 to the complete absence of the enzyme.

245

246 ***Both Deletion and Overexpression of MiaA Increase Frameshifting***

247 Previous research in K-12 *E. coli* and *Salmonella* showed that deletion of *miaA*
248 can compromise translational fidelity, resulting in increased ribosomal frameshifting [73,
249 74]. To determine the effects of MiaA on frameshifting in UT189, we utilized dual-luciferase
250 reporter plasmids that consist of a translational fusion of firefly luciferase downstream of
251 renilla luciferase. Linker sequences, derived from either Antizyme 1 (Az1) or HIV *gag-pol*,
252 were placed between the two luciferase genes (**Fig. 6A**). The Az1-derived linker
253 sequence contains a stop codon positioned in-frame so that a +1 frameshift must occur
254 for read-through expression of firefly luciferase [75]. In contrast, a -1 frameshift is required
255 for expression of firefly luciferase downstream of the HIV-derived linker [76]. Importantly,
256 upstream of the in-frame stop codons in both linkers are UNN codons that can be
257 recognized by MiaA-modified tRNAs. The firefly and renilla luciferases act on distinct
258 substrates, which are used to sequentially assess levels of expression of each enzyme
259 [75, 76]. Control plasmids in which the two luciferases are in-frame were used to
260 normalize the data by accounting for ribosome drop-off.

261 To examine the consequences of MiaA expression on frameshifting, the dual-
262 luciferase reporter constructs were used in combination with wild-type UT189,
263 UT189 Δ *miaA*, UT189/pMiaA_{P_{tac}}, and UT189 carrying the empty control vector pRR48. After
264 overnight growth in LB, UT189 and UT189 Δ *miaA* were back-diluted into LB while
265 UT189/pMiaA_{P_{tac}} and UT189/pRR48 were back-diluted into LB + 1 mM IPTG to induce
266 MiaA expression. After reaching mid-log growth, the enzymatic activities of the two
267 luciferases were quantified. Both the lack of MiaA and MiaA overexpression caused
268 notable increases in frameshifting in both the +1 and -1 directions (**Fig. 6B-C**). These

269 results confirm that loss of MiaA can increase frameshifting and show that elevated MiaA
270 levels can likewise impact the fidelity of translation.

271

272 ***Changing levels of MiaA alters the spectrum of expressed proteins***

273 To determine how deletion and overexpression of MiaA affect translation we used
274 multidimensional protein identification technology (MudPIT; LC-MS/MS) with wild-type
275 UTI89 and UTI89 Δ *miaA* cultures grown to mid-log phase in LB, and UTI89/pMiaA_{P_{ta}c} and
276 UTI89/pRR48 similarly grown in LB + 1mM IPTG. Of 1,524 proteins detected in UTI89
277 and UTI89 Δ *miaA*, 105 were picked up only in the wild-type strain and 23 were unique to
278 the *miaA* knockout mutant (**Fig. 7A**). 1,471 proteins were identified in UTI89/pRR48 and
279 UTI89/pMiaA_{P_{ta}c}, with 42 being exclusive to UTI89/pRR48 and 20 seen only in the MiaA
280 overexpression strain (**Fig. 7B**). 115 proteins were significantly downregulated in
281 UTI89 Δ *miaA* relative to wild-type UTI89, while 34 proteins were upregulated in the
282 knockout mutant (**Fig. 7C**). Notably fewer proteins were significantly altered when MiaA
283 was overexpressed. Relative to the control strain UTI89/pRR48, 20 proteins were
284 downregulated in UTI89/pMiaA_{P_{ta}c}, whereas nine (including MiaA) were upregulated (**Fig.**
285 **7D**).

286 The specific proteins detected, including those that were differentially expressed
287 due to *miaA* deletion or overexpression, are detailed in **Supplemental Dataset S1**. The
288 differentially expressed proteins were assigned to one or more of 14 functional categories
289 (see *Categories* worksheet and embedded graph in **Supplemental Dataset S1**). A
290 majority of the altered proteins were linked with metabolic pathways, secondary
291 metabolites, and functions associated with the bacterial envelope. These included several

292 proteins involved in sugar and fatty acid metabolism and the biosynthesis and regulation
293 of electron transport chains (e.g. UbiC, WrbA, ChrR, Qor, NuoM, NudJ, and CyoC). The
294 dysregulation of these factors likely contributed to the various phenotypic defects
295 observed in our *in vitro* and *in vivo* assays and suggested MiaA involvement in other
296 important processes.

297 In particular, many of the differentially expressed proteins were shown in previous
298 studies to directly or indirectly affect motility or biofilm development. The former group
299 comprised the chemotaxis protein CheA and the flagella-associated proteins FlhF, FlhA,
300 and FlgH. Not unexpectedly, both deletion of the *miaA* gene and MiaA overexpression
301 markedly decreased UTI89 motility on swim plates (**Supplemental Fig. S6**). MiaB did not
302 affect motility in these assays. Factors linked with biofilm development include YoaB, the
303 type 1 pilus-associated regulator FimB and periplasmic chaperone FimC, the acid stress-
304 response chaperone HdeB, the cellulose synthase catalytic subunit BcsA, and the
305 cytochrome *bo* subunit CyoC. Using yeast extract-casamino acids (YESCA) medium,
306 which promotes the development of elaborate rugose-colony biofilms [77, 78], we found
307 that UTI89 Δ *miaA*, but not UTI89 Δ *miaB*, formed atypical biofilms with notably less rugosity
308 than the parent strain (**Fig. 8**). Interestingly, the biofilms formed by UTI89 Δ *miaA* were
309 architecturally similar to those formed by a UTI89 mutant lacking the CyoC-interacting
310 partners CyoAB [78].

311 Our MudPIT results also indicated that MiaA can regulate numerous proteins that
312 have been associated with redox and bacterial responses to nitrosative, oxidative, and
313 more generally, genotoxic stresses (**Supplemental Dataset S1**). Aberrant expression of
314 these factors, including proteins like GadB, CadA, Dps, glutathione S-transferase Gst,

315 and the glutathione reductases GrxB and GrxC, may account for increased sensitivity to oxygen
316 and nitrogen radicals (see **Fig. 2D-H** and **Fig. 5D and F**). Some of these factors, and
317 others like HdeA and HdeB, can also guard against acid stress. Accordingly, follow-up
318 experiments confirmed that UTI89 Δ *miaA*, but not UTI89 Δ *miaB*, is notably less resistant
319 to acid stress than the wild-type strain (**Supplemental Fig. S7**). On average, relative to
320 wild-type UTI89, UTI89 Δ *miaA* titers were reduced over 6,000-fold following exposure to
321 acidic conditions in LB.

322 The sensitivity of both UTI89 Δ *miaA* and UTI89/pMiaA_{P_{tac}} to osmotic stress may
323 arise due to the significant downregulation of proteins like SLP, BetB, YggT, ProP, and
324 YnaI (**Supplemental Dataset S1**). Other differentially expressed proteins that probably
325 contribute to the varied phenotypes associated with *miaA* deletion or MiaA
326 overexpression in our assays include multiple transcriptional regulators, several
327 ribosome- and RNA-associated factors, and the tRNA ligases LysU, TyrS, and PheS.
328 These findings indicate that MiaA is tied into a complex web of factors that can have direct
329 and indirect effects on translation. Driving this point home is the observation that MiaA
330 overexpression suppresses the production of TadA, an enzyme that catalyzes the
331 deamination of adenosine-to-inosine (A-to-I) in Arg2 tRNA and a select set of mRNAs
332 [79, 80]. In K-12 *E. coli*, the A-to-I editing function of TadA can recode at least 12 mRNAs,
333 which results in the generation of proteins with altered activities that can impact bacterial
334 cell physiology [80]. Among the known TadA-edited transcripts is one encoding IlvC, an
335 enzyme involved in isoleucine and valine biosynthesis which, like TadA, is downregulated
336 ~3.5-fold in UTI89 when MiaA is overexpressed (**Fig. 7D**).

337

338 ***UTI89* Δ *miaA* phenotypes are not entirely due to aberrant RpoS or Hfq expression**

339 In K-12 *E. coli*, the deletion of *miaA* results in decreased translation of the alternate
340 Sigma factor RpoS (σ^S) and the small RNA chaperone Hfq [7, 30, 31]. Both of these
341 factors are important for the stress resistance and virulence potential of ExPEC [62, 81].
342 In line with results from K-12 *E. coli*, our proteomics analysis indicated that RpoS and Hfq
343 levels were reduced 2.5- and 2.8-fold, respectively, in *UTI89* Δ *miaA* relative to the wild-
344 type strain (**Fig. 7C** and **Supplemental Dataset S1**). RpoS downregulation in the
345 absence of *miaA* was also confirmed by western blot analysis (**Supplemental Fig. S8A**)
346 These observations suggest that the phenotypic defects associated with *UTI89* Δ *miaA*
347 might be attributable to aberrant expression of RpoS or Hfq. However, despite some
348 similarities, the phenotypes that we previously observed with *UTI89* mutants lacking
349 either *rpoS* or *hfq* are distinct from one another and from those that we report here with
350 *UTI89* Δ *miaA* [62, 81]. Furthermore, the induced expression of recombinant RpoS or Hfq
351 (**Supplemental Fig. S8B and C**) failed to rescue growth of *UTI89* Δ *miaA* under
352 hyperosmotic conditions (**Supplemental Fig. S8D and E**). The pRpoS_{P_{tac}} and pHfq_{P_{tac}}
353 expression constructs used in these assays can complement *UTI89* mutants lacking *rpoS*
354 or *hfq*, respectively [62, 81]. Cumulatively, these data indicate that the phenotypes seen
355 with *UTI89* Δ *miaA* are not entirely due to attenuated expression of either RpoS or Hfq.
356 Also of note, our ability to complement *UTI89* Δ *miaA* with *MiaA* expression constructs (see
357 **Figs. 2, 3, and 8**) demonstrates that the phenotypic defects associated with this knockout
358 mutant are not caused by off target mutations or polar effects on *hfq*, which lies
359 immediately downstream of *miaA*.

360

361 ***UNN-Leu codon usage by MiaA-sensitive transcripts***

362 Messages like those encoded by *rpoS* and *hfq* are classified as Modification
363 Tunable Transcripts (MoTTs), which are identifiable by 1) codon usage different from that
364 of average transcripts and 2) translation that is sensitive to changing levels of tRNA
365 modifications [31, 82]. Studies in the K-12 *E. coli* strain MG1655 of *rpoS*, *hfq*, and other
366 transcripts suggest that MiaA-sensitive MoTTs have higher than average ratios of UNN-
367 Leu codons relative to total Leu codons [30, 31]. This led us to ask if UNN-Leu codon
368 usage correlates with protein expression levels in UTI89 when MiaA is either absent or
369 over-produced. Plotting results from our MudPIT analysis versus UNN-Leu codon usage
370 (**Supplemental Dataset S1**) showed that just over 60% of the proteins that are
371 differentially expressed in UTI89 Δ *miaA* or UTI89/pMiaA_{P_{tac}} have UNN-Leu codon usage
372 ratios that are greater than the K-12 average ratio of 0.22 (**Fig. 9**, green dashed line). In
373 line with previous findings [30, 31], RpoS and Hfq are among the differentially expressed
374 proteins with UNN-Leu codon usage ratios of greater than 0.22. However, the average
375 UNN-Leu codon usage ratio in UTI89 is somewhat higher than that in K-12 *E. coli*. Using
376 this value, which is 0.28, less than half of the proteins that are differentially regulated in
377 UTI89 Δ *miaA* or UTI89/pMiaA_{P_{tac}} have greater than average UNN-Leu codon usage ratios
378 (**Fig. 9**, black dashed line). Furthermore, among the proteins that are not significantly
379 altered by either deletion or overexpression of *miaA*, about 30% have UNN-Leu codon
380 usage ratios greater than 0.28. Cumulatively, these data indicate that UNN-Leu codon
381 ratios alone may not be especially useful for predicting MiaA-sensitive protein expression
382 patterns within ExPEC strains like UTI89.

383

384 DISCUSSION

385 The results presented here demonstrate that MiaA is crucial for ExPEC fitness and
386 virulence, and that changing MiaA levels can impact the translation of a broad spectrum
387 of proteins. Our findings are in line with previously published work showing that tRNA
388 modifying enzymes can influence the virulence potential of a variety of microbial
389 pathogens [83]. The attenuation of bacterial virulence-related phenotypes in the absence
390 of a specific tRNA modifying enzyme can, in some cases, be explained by sub-optimal
391 translation of specific toxins or key regulatory factors [14, 19-21]. For example, deletion
392 of *miaA* in the diarrheagenic bacteria *Shigella flexneri* ablates translation of the
393 transcriptional master regulator VirF, resulting in the reduced expression of downstream
394 virulence factors [11, 84]. Overexpression of recombinant VirF alone is sufficient to rescue
395 the *miaA* mutant, suggesting that low-level production of VirF is in large part responsible
396 for the virulence-related defects caused by the deletion of *miaA* in *S. flexneri*. In contrast,
397 our work indicates that the diverse phenotypes affected by MiaA expression in the ExPEC
398 isolate UTI89 are not attributable to any single factor, but rather arise due to the altered
399 expression and dysregulation of multiple proteins and pathways downstream of MiaA.

400 The ms²i⁶A modification is understood to affect the fidelity of translation [5, 8, 27].
401 Earlier work in K-12 *E. coli* and *Salmonella* strains showed that bacteria lacking *miaA*
402 have an increase in the +1 direction of frameshifting, but not the -1 direction [73, 74]. In
403 these studies, the i⁶A modification was found to be a major contributor to ribosome fidelity.
404 In UTI89, significant increases in frameshifting were seen in both the +1 and -1 directions
405 when *miaA* was knocked out. When MiaA was overproduced, we also observed marked
406 elevation of frameshifting in the -1 direction, while frameshifting levels in the +1 direction

407 were more modest. Most reports to date indicate that tRNA modifications typically affect
408 frameshifting primarily in one direction [5, 74]. At first glance, our data seemingly counter
409 this trend. However, we note that the expression of firefly luciferase downstream of the
410 HIV-derived linker in our reporter system may also occur as a consequence of a +2
411 frameshift, rather than a -1 frameshift, which would more closely mirror what was
412 observed in previous studies with K-12 *E. coli* and *Salmonella* strains [73, 74]. It is also
413 possible that the apparent increases in both -1 and +1 frameshifting observed in our
414 assays reflect the presence of MiaA-sensitive regulatory circuits in UTI89 that are different
415 from those in K-12 *E. coli* or *Salmonella* strains.

416 During the course of this study, we were surprised to observe that MiaA levels in
417 the ExPEC reference strain UTI89 were substantially decreased in response to high salt
418 (see **Fig. 4**). Ongoing work indicates that MiaA levels in UTI89 are also altered upon
419 exposure to other stressors, such as MV (**Supplemental Fig. S9A and B**). Due to the
420 sweeping phenotypes seen in the absence of MiaA, we hypothesized that the levels of
421 MiaA would have stayed the same or increased in response to stressors like high salt and
422 MV. However, our data indicate that MiaA levels are fine-tuned within ExPEC such that
423 too much or too little enzyme can have similarly detrimental consequences. The effects
424 of MiaA expression in our growth curve assays were dose-dependent, with high-level
425 expression of MiaA being nearly as disruptive as the deletion of *miaA*. For instance, low-
426 level expression of MiaA restored the resistance of UTI89 Δ *miaA* to high salt, whereas
427 overexpression of MiaA resulted in greatly increased sensitivity (see **Fig. 5**).

428 MiaA is part of a complex superoperon and its regulation, and the regulation of
429 tRNA modifying enzymes in general, is not well understood [33, 85, 86]. Though we did

430 not investigate MiaA regulation in detail here, our RT-qPCR experiments indicate that
431 MiaA levels are reduced in response to high salt stress via a post-transcriptional
432 mechanism (**Fig. 4C**). Interestingly, *miaA* has a higher-than-average UNN Leu codon
433 usage ratio of 0.46, suggesting that MiaA may help regulate the translation of its own
434 transcripts [31]. Furthermore, we note that MiaA levels are intensified in the presence of
435 the metal chelator EDTA (**Supplemental Fig. S9C**), raising the possibility that the
436 quantities of this tRNA modifying enzymes are controlled by one or more EDTA-sensitive
437 metalloproteases. The factors that modulate MiaA levels during times of stress require
438 further investigation.

439 By adjusting the levels of tRNA modifying enzymes like MiaA, ExPEC and other
440 organisms may be able to vary the diversity of translated proteins and thereby optimize
441 adaptive responses to stressful stimuli [14, 33, 46, 87-90]. Indeed, the overexpression
442 and deletion of *miaA* led to the generation of distinct proteomes by UT189 (**Fig. 7**) and
443 compromised the ability of this ExPEC strain to deal with multiple stressors. Because
444 tRNA modifications can have pleiotropic effects, it is not always easy to distinguish the
445 direct and indirect effects that tRNA modifying enzymes like MiaA have on translation
446 [90]. For example, pioneering work in K-12 *E. coli* indicates that the efficient translation
447 of RpoS and Hfq relies on MiaA for proper decoding of UNN-Leu codons [7, 30, 31], but
448 these factors can themselves regulate the expression of numerous other proteins [91-93].
449 The capacity for MiaA to have additional, indirect effects on the fidelity and specificity of
450 translation is further highlighted by our proteomics data showing that MiaA impacts the
451 expression of multiple ribosome- and RNA-associated factors, tRNA ligases, and the RNA
452 editing enzyme YfhC (TadA). These findings suggest the existence of a complex network

453 of RNA and translational modifiers that can regulate the expression of one another.
454 Layered on top of this is the potential for MiaA to affect the biosynthesis and availability
455 of specific metabolites used by other tRNA modifying enzymes [15, 33].

456 Increases in frameshifting due to changing levels of MiaA may also allow for more
457 error-prone translation and the subsequent diversification of expressed proteins, which
458 could allow bacteria to better deal with stressful stimuli. The ability of cells to actively
459 regulate frameshifting and other translational errors in order to generate mutant proteins
460 that deviate from those encoded by the genome is gaining appreciation as an adaptive
461 response to stress [94-97]. Ongoing studies aim to utilize ribosomal profiling along with
462 RNA-seq and proteomics to determine if off-frame and mutant proteins are being
463 produced by ExPEC via translational modifiers like MiaA in response to stressful stimuli.
464 Similar lines of research may also shed light on the somewhat more cryptic functions of
465 the MiaB-catalyzed tRNA modification.

466 In the absence of *miaA*, the i^6A and ms^2i^6A modifications are not detectable (**Fig.**
467 **4**), as expected from previously published work [86]. When MiaA is overproduced, high
468 levels of i^6A are observed, while ms^2i^6A modification levels remain relatively stable (**Fig.**
469 **5A**). This suggests that only a fraction of the UNN-decoding tRNAs are fully modified in
470 the cell at any time. Interestingly, high salt stress reduces both MiaA expression and
471 ms^2i^6A levels, but does not significantly affect i^6A levels (**Fig. 4**). In contrast, the disruption
472 of *miaB* prevents the formation of ms^2i^6A and causes marked increases in i^6A levels
473 (**Supplemental Fig. S4**), but this had no phenotypic effect in any of our assays. These
474 findings present a conundrum – why does high-level production of i^6A due to MiaA
475 overexpression attenuate the stress resistance of UTI89 while even higher levels of i^6A

476 that build up in the absence of MiaB had no overt phenotypic effects in our assays? In
477 considering this issue, it should be noted that we quantified relative levels of i⁶A and
478 ms²i⁶A, and not specific tRNAs, leaving open the possibility that changing levels of MiaA
479 differentially affect distinct tRNA subsets. This alone could account for the contrasting
480 phenotypic effects linked with elevated i⁶A levels due to MiaA overexpression versus
481 those caused by *miaB* deletion. MiaA overexpression may also be detrimental due to
482 depletion of substrates like dimethylallyl diphosphate (DMAPP) that feed into other critical
483 pathways, including the biosynthesis of ubiquinone. The deletion of *miaB*, by causing a
484 buildup of i⁶A rather than accelerated production of this modified residue, may have less
485 of an abrupt impact on the availability substrates like DMAPP. Finally, it is feasible that
486 MiaA has moonlighting function(s), affecting non-tRNA targets and compromising
487 bacterial fitness when produced in excess. Cumulatively, the findings presented here
488 highlight the central and complex roles that core metabolic genes like *miaA* can have on
489 the elaboration and fine-tuning of pathogen stress resistance and virulence-associated
490 phenotypes.

491

492 **EXPERIMENTAL PROCEDURES**

493 ***Bacterial strains.*** Strains used in this study are listed in **Supplemental Table S1**. Mutant
494 strains were constructed in the reference ExPEC isolate UTI89 using the lambda Red
495 recombination system and primers detailed in **Supplemental Table S2**, as previously
496 described [48]. The chloramphenicol resistance (CIm^R) cassette flanked by LoxP sites
497 was amplified from plasmid pKD3 using primers that contain overhanging ends with ~40
498 bp of homology near the 5' and 3' ends of each target locus. PCR products were

499 introduced by electroporation into UTI89 carrying pKM208, which encodes an IPTG-
500 inducible lambda Red recombinase [49]. Knockouts were verified by PCR using primers
501 indicated in **Supplemental Table S2**.

502

503 **Plasmids.** Expression and reporter constructs were generated using standard molecular
504 biology approaches and primers listed in **Supplemental Table S2**. The *miaA* and *miaB*
505 genes were amplified from UTI89 by PCR, digested, and ligated into pRR48 using Pst1
506 and Kpn1 restriction sites to create pMiaA_{P_{tac}} and pMiaB_{P_{tac}}. Sequences encoding Hfq
507 fused with C-terminal 6xHis and Flag tags were cloned using a similar approach to make
508 pHfq_{P_{tac}}. To create pMiaA_{nat}, the UTI89 *miaA* sequence was amplified along with 200
509 base pairs of flanking sequences, including the *miaA* promoter, and then ligated into the
510 EcoR1 site of pACYC184. The plasmid pMiaA-Flag_{nat}, having the *miaA* promoter region
511 upstream of sequences encoding MiaA with a C-terminal Flag-tag, was produced
512 similarly.

513 The dual-luciferase reporter plasmids used for the frameshifting assays were
514 created using p2Luc plasmids as templates [75, 76]. The genes encoding the renilla and
515 firefly luciferases were amplified by PCR along with intergenic Az1- or HIV-derived linker
516 sequences. A Shine-Dalgarno ribosome binding site was incorporated into the forward
517 primer (p2Luc_F) primer to promote translation of the linked luciferases. PCR products
518 were digested and ligated into the KpnI and HindIII sites of pBAD18 (Ap^R) and pBAD33
519 (Cam^R). Plasmids with different resistance cassettes were needed for use with
520 UTI89Δ*miaA* (Cam^R) and UTI89 carrying pMiaA_{P_{tac}} or the empty vector pRR48. The Az1-
521 and HIV-derived linker region sequences are noted in **Fig. 6A**, and were chosen because

522 they contain MiaA-sensitive UNN codons. Control plasmids in which the Az1 and HIV
523 linkers are altered to place the two luciferases in-frame were generated in an analogous
524 fashion using previously described p2Luc plasmids as templates [75, 76].

525

526 **Bacterial growth analysis.** UTI89 and its derivatives were grown from frozen stocks in
527 5 ml of LB, 100 mM MES-buffered LB (MES-LB; pH 5.0), or modified M9 medium (6 g/liter
528 Na₂HPO₄, 3 g/l KH₂PO₄, 1 g/l NH₄Cl, 0.5 g/l NaCl, 1 mM MgSO₄, 0.1 mM CaCl₂, 0.1%
529 glucose, 0.0025% nicotinic acid, 0.2% casein amino acids, and 16.5 µg/ml thiamine in
530 H₂O) at 37°C overnight in loosely capped 20-by-150-mm borosilicate glass tubes with
531 shaking (225 rpm, with tubes tilted at a 30° angle). Overnight cultures were brought to an
532 OD₆₀₀ of ~1.0 and then sub-cultured 1:100 into LB, MES-LB, or M9 medium. Growth
533 curves were acquired using a Bioscreen C instrument (Growth Curves USA) with 200-µl
534 cultures in 100-well honeycomb plates shaking at 37°C. Cultures included extra NaCl (5%
535 w/v), 1 mM MV (Sigma-Aldrich), 1 or 2 mM ASN (Sigma-Aldrich), or IPTG, as indicated.
536 MV and ASN solutions were prepared fresh just before use. All growth curves were
537 determined using quadruplicate samples with at least three independent replicates.
538 Overnight cultures of strains carrying plasmids for complementation experiments were
539 grown in the presence of antibiotics (100 µg of ampicillin/ml or 50 µg of tetracycline/ml)
540 to maintain the plasmids, but antibiotics were not included in media used for the
541 subsequent growth assays.

542

543 **Mouse models.** All animals used in this study were handled in accordance with protocols
544 approved by the Institutional Animal Care and Use Committee at the University of Utah

545 (Protocol number 10-02014), following US federal guidelines indicated by the Office of
546 Laboratory Animal Welfare (OLAW) and described in the Guide for the Care and Use of
547 Laboratory Animals, 8th Edition. Mice were purchased from The Jackson Laboratory,
548 housed 3 to 5 per cage, and allowed to eat (irradiated Teklad Global Soy Protein-Free
549 Extruded chow) and drink antibiotic-free water *ad libitum*.

550 *Competitive gut colonization assays.* For these assays, a kanamycin resistance
551 cassette (Kan^R) was inserted into the *attTn7* site of UTI89 to create UTI89::Kan^R, which
552 can be easily distinguished from the chloramphenicol resistant (Cam^R) *miaA* and *miaB*
553 knockout mutants by plating on selective media. Previous work demonstrated that
554 insertion of resistance cassettes into the *attTn7* site does not impact ExPEC fitness within
555 the gut [55, 56]. Individual cultures of UTI89::Kan^R (standing in as the wild-type strain),
556 UTI89Δ*miaA*, and UTI89Δ*miaB* were grown statically from frozen stocks for 24 h at 37°C
557 in 250-ml flasks containing 20 ml of modified M9 medium. Each knockout mutant was
558 then mixed 1:1 with UTI89::Kan^R (6 ml of each culture) and then pelleted by centrifugation
559 at 8,000 x *g* for 8 minutes at room temperature. The bacterial pellets were then washed
560 once with phosphate-buffered saline (PBS), pelleted again, and resuspended in 0.5 ml of
561 PBS. Female SPF BALB/c mice aged 7 to 8 weeks were inoculated via oral gavage with
562 50 μl PBS containing ~10⁹ CFU of each bacterial mixture. At the indicated time points
563 post-inoculation, individual mice were placed into unused takeout boxes for a few minutes
564 for weighing and feces collection. Freshly deposited feces were collected from the boxes
565 and immediately added to 1 ml of 0.7% NaCl, weighed, and set on ice. The samples were
566 then homogenized and briefly centrifuged at low speed to pellet any insoluble debris.
567 Supernatants were serially diluted and plated onto LB agar containing either

568 chloramphenicol (20 µg/ml) or kanamycin (50 µg/ml) for selective growth of UTI89::Kan^R
569 (wild type), UTI89Δ*miaA*, or UTI89Δ*miaB*. Fecal samples were also analyzed prior to the
570 start of each experiment to ensure that there were no endogenous bacteria present that
571 were resistant to chloramphenicol or kanamycin. CIs were calculated as the ratio of
572 knockout over wild-type bacteria recovered in the feces divided by the ratio of knockout
573 over wild-type bacteria present in the inoculum [55, 57]. A total of 7 to 8 mice in two
574 independent assays were used for each set of bacterial strains tested.

575 *UTI model.* The murine UTI model was used essentially as described by our group
576 and others [98, 99]. Wild-type UTI89 and the *miaA*, and *miaB* knockout mutants were
577 grown from frozen stocks in 20 ml LB broth in 250 mL Erlenmeyer flasks without shaking
578 at 37°C for 24 hours. Bacteria were then pelleted by centrifugation (8 minutes at 8,000 x
579 g) and resuspended in PBS. Seven- to eight-week-old female CBA/J or C3H/HeJ mice
580 were briefly anesthetized by isoflurane inhalation and slowly inoculated via transurethral
581 catheterization with 50 µL of PBS containing a suspension of ~10⁷ bacteria. Bacterial
582 reflux into the kidneys using this procedure is rare, occurring in less than 1% of the test
583 animals. At 0.25, 1, 3, or 9 days post-inoculation, mice were sacrificed and bladders were
584 harvested aseptically, weighed, and homogenized in 1 ml PBS containing 0.025% Triton
585 X-100. Bacterial titers within the homogenates were determined by plating serial dilutions
586 on LB agar plates. Nine or more mice in total, from two independent experiments, were
587 used for each bacterial strain and time point examined.

588 *Sepsis model.* UTI89, UTI89Δ*miaA*, and UTI89Δ*miaB* were grown from frozen
589 stocks in 20 ml M9 broth without shaking at 37°C for 24 h, pelleted by centrifugation at
590 8,000 x g for 8 minutes, and washed once with PBS, pelleted again, and resuspended in

591 PBS. Seven- to eight-week-old female C57Bl/6 mice were briefly anesthetized by
592 isoflurane inhalation and infected via intraperitoneal injection of $\sim 10^7$ CFU within 200 μ l
593 PBS. Mice were monitored over a 72-hour period for signs of morbidity and mortality.
594 Alternatively, at 6 hours post-inoculation mice were sacrificed and the liver, kidneys, and
595 spleens were harvested aseptically, weighed, and homogenized in 1 ml PBS containing
596 0.025% Triton X-100. Bacterial titers within the homogenates were determined by plating
597 serial dilutions on LB agar plates.

598

599 ***Invasion, adhesion, and intracellular persistence assays.*** Bacteria were grown at
600 37°C for 48 h in 20 mL static LB broth to induce expression of type 1 pili, which are
601 important mediators of UPEC adherence and entry into host cells [99]. Host cell
602 association and gentamicin protection-based invasion and overnight intracellular
603 persistence assays were performed as previously described using the human bladder
604 epithelial cell line 5637 (HTB-9; ATCC) [100]. Of note, UTI89 $\Delta miaA$ is about 3-fold more
605 sensitive to the host-cell impermeable antibiotic gentamicin, as determined by using
606 Etest Strips (VWR) (**Supplemental Fig. S10**). However, this likely had no effect on
607 results from the cell culture-based invasion and intracellular survival experiments, as the
608 concentrations of gentamicin (100 and 10 μ g/ml) used in these assays exceed those
609 needed to effectively kill extracellular UTI89, UTI89 $\Delta miaB$, and UTI89 $\Delta miaA$.

610

611 ***Biofilm analysis.*** *In vitro* rugose biofilm assays were performed starting with cultures
612 grown overnight at 37°C shaking in LB, as described [78]. Bacteria from each culture
613 were then brought to an OD₆₀₀ of ~ 1.0 and 10 μ l aliquots were spotted onto YESCA agar

614 plates (12 g/l Casamino acids, 1.2 g yeast extract, 22 g agar) and incubated at RT (~20-
615 22°C). After 14 days, biofilm images were acquired by focus stacking using an M.Zuiko
616 Digital ED 60 mm lens mounted on an Olympus OM-D E-M1 Mark II camera.

617

618 **Motility assays.** Cultures of UTI89, UTI89 Δ *miaA*, and UTI89 Δ *miaB* grown overnight
619 shaking in LB or M9 medium were brought to OD₆₀₀ of 1.0. Swim motility plates, containing
620 0.2% agar in LB or M9 medium, were inoculated with 2 μ l of each bacterial suspension
621 delivered just below the agar surface. The diameter of bacterial spreading was measured
622 every 1-2 hours over the course of an 8-10 hour-incubation at 37°C. Swim rates were
623 calculated during logarithmic growth. To assess the effects of MiaA and MiaB
624 overexpression on motility, tryptone soft agar plates [101] containing 50 μ g/ml ampicillin
625 and 100 μ M IPTG were inoculated with UTI89/pRR48, UTI89/pMiaA_{P_{tac}}, and
626 UTI89/pMiaB_{P_{tac}} from overnight shaking cultures. Plates were imaged after a 6-hour
627 incubation at 37°C.

628

629 **Acid resistance assays.** Bacterial strains from overnight cultures were diluted 1:100 in
630 fresh LB and grown shaking at 37°C for 3 h. Concentrated HCl was then added to each
631 culture to adjust the pH to 3.0 and incubations were continued for another 30 minutes.
632 Bacteria from 1 ml of each culture were then pelleted at 16,000 x g for 5 min and washed
633 in PBS. Surviving bacteria were enumerated by plating serial dilutions on LB agar and
634 normalized to input titers.

635

636 **Osmotic stress resistance assays.** UTI89/pACYC184, UTI89 Δ *miaA*/pACYC184,
637 UTI89 Δ *miaA*/pMiaA_{nat}, and UTI89 Δ *miaB* were grown shaking overnight at 37°C in 5 ml
638 LB broth with 20 µg/ml tetracycline and then back diluted 1:100 into 5 ml fresh LB (+
639 tetracycline). After 5 h shaking at 37°C, a 1-ml aliquot of each culture was pelleted,
640 resuspended in 1 ml of sterile water with or without 0.1% glucose, and incubations were
641 continued for another 2 h with shaking at 37°C. Viable bacteria present at 0, 30, 60, 90,
642 and 120 min after resuspension in water were quantified by dilution plating and
643 normalized to input titers. Growth curves in LB \pm 5% NaCl were acquired as described
644 above.

645
646 **Western blot analysis.** Bacterial pellets were frozen at -80°C and then resuspended in
647 B-PER lysis reagent (Thermo Scientific) supplemented with 1 mM phenylmethylsulfonyl
648 fluoride, protease inhibitor cocktail (Roche), and Lysonase Bioprocessing Reagent
649 (Novagen). After a 15-minute incubation at room temperature, samples were spun for 1
650 minute at 13,000 x g to remove large cell debris, and protein concentrations in the
651 supernatants were determined using the BCA reagent system (Pierce). Equivalent protein
652 amounts were resolved by SDS-PAGE and subsequently transferred to Immobilon PVDF-
653 FL membranes (Millipore). Blots were probed using mouse anti-Flag M2 (1:3000; Sigma-
654 Aldrich), rabbit anti-Flag (Immunology Consultants laboratory, inc.), and mouse anti-
655 RpoS (anti-SigmaS; Biolegend) and visualized using enhanced chemiluminescence with
656 HRP-conjugated secondary antibodies (1:3000 or 1:5000; Amersham Biosciences), as
657 described [102]. To ensure that equivalent amounts of protein from each sample were
658 analyzed, blots were re-probed using rabbit anti-*E. coli* antisera (1:2,000 or 1:5000;
659 BioDesign International).

660

661 **Analysis of relative *i6A* and *ms2i6A* levels.** UTI89 and UTI89 Δ *miaA* were grown from
662 frozen stocks shaking at 37°C overnight in LB. UTI89/pRR48 and UTI89/pMiaA_{P_{tac}} were
663 grown similarly using LB supplemented with ampicillin (100 µg/ml). The bacteria were
664 sub-cultured 1:100 into 6 ml of LB ± 1 mM IPTG and then grown shaking to an OD₆₀₀ of
665 0.5. After adjusting the cultures to OD₆₀₀ of 1.0, the bacteria were pelleted by spinning
666 at 8000 x g for 1.5 minutes. Pellets were then resuspended in 1 ml of RNA_{later}
667 Stabilization Solution (ThermoFisher) and stored at 4°C overnight prior to extraction of
668 RNA using a Norgen Total RNA Extraction Kit.

669 Samples were analyzed using a Hypersil GOLD C18 column (2.1 mm × 150 mm,
670 1.9 µm particle size; Thermo Fisher) attached to a Thermo Scientific Dionex UltiMate
671 3000 UHPLC instrument in line with an LTQ-Orbitrap XL instrument (Thermo Fisher).
672 The LC-MS parameters were based upon a procedure described previously [103, 104],
673 with the following adjustments. The UHPLC column was pre-equilibrated in 100% Buffer
674 A [50 mM ammonium acetate (Fisher) in LC-MS Optima water]. Buffer B consisted of
675 60% (v/v) LC-MS Optima acetonitrile (Fisher) and 40% LC-MS water (Fisher). The
676 reaction components were eluted at a rate of 0.2 ml/minute with the following program:
677 0% B from 0 to 3.46 min, 0 to 0.9% B from 3.46 to 3.69 min, 0.9 to 1.5% B from 3.69 to
678 3.92 min, 1.5 to 3% B from 3.92 to 4.25 min, 3 to 20% B from 4.25 to 6.5 min, 20 to 25%
679 B from 6.5 to 7 min, 25 to 40% B from 7 to 8.5 min, 40 to 45% B from 8.5 to 9.25 min,
680 45 to 60% B from 9.25 to 9.95 min, 60 to 100% B from 9.95 to 10.45 min, 100% B from
681 10.45 to 16 min, 100 to 0% B from 16 to 16.1 min, and 0% B from 16.1 to 20 min. The

682 flow from the column was diverted to the mass spectrometer from 3.5 minutes to 17
683 minutes during the UHPLC program. The mass spectrometer was operated in positive
684 ion mode, and authentic guanosine material (Sigma Aldrich) was used to generate a
685 tune file for the instrument. The observed m/z values of the +1 charge states of the i6a
686 and ms2i6a RNA bases were 336.1658 and 382.1535, respectively. The observed
687 retention times for i6A and ms2i6a were determined from the center of their extracted
688 ion chromatogram peaks to be 15.55 and 16.45 minutes, respectively. The retention
689 time of i6a from biological extracts was consistent with the retention time of authentic
690 i6a material (Cayman Chemical). Absolute intensities of the i6a ions were retrieved from
691 the mass spectrum scanned between 15.4 – 16.1 minutes, while the absolute intensities
692 of the ms2i6a ions were retrieved from the mass spectrum scanned between 16.2 and
693 17.0 minutes. The scan range was chosen to include the entire peak of an EIC trace,
694 excluding mass spectral data recorded out of these bounds. This ensured that the
695 intensities of ions 336.17 and 382.15 arise from eluted i⁶A and ms²i⁶A material and did
696 not include background during the rest of the run. The scan windows were wide enough
697 to account for any small drift in retention that might occur from sample to sample.
698 Because total RNA concentration varied by sample, the samples were normalized
699 against the total RNA concentration of each sample, as estimated via a NanoDrop
700 measurements at 260 nm.

701 **Quantification of frameshifting.** UTI89, UTI89 Δ *miaA*, UTI89/pRR48 and
702 UTI89/pMiaA_{P_{tac}} carrying one of the dual-luciferase reporter plasmids (see
703 **Supplemental Table S1**) were grown overnight in LB supplemented with
704 chloramphenicol (20 μ g/ml) or ampicillin (100 μ g/ml). The cells were sub-cultured 1:100

705 into 6 ml LB with and without 1mM IPTG. At an OD₆₀₀ of 0.2, arabinose (0.2%) was
706 added to all of the cultures to induce expression of the luciferases. Cells were allowed
707 to continue growing until reaching an OD₆₀₀ of 0.5, at which point the cultures were
708 adjusted to an OD₆₀₀ of 1.0 and pelleted by spinning at 8000 x g for 1.5 minutes. The
709 pellets were then subjected to one freeze-thaw cycle before being resuspended in
710 Passive Lysis Buffer (Promega; E1910). One scoop of 0.15 mm zirconium oxide beads
711 (Next Advance; ZrOB015) was added to each tube and bacteria were lysed using a
712 Bullet Blender (Next Advance) set at speed 8 for 3 min. After a 30-second spin in a
713 microfuge to pellet beads and any large debris, the supernatants were collected and
714 luciferase activities were analyzed as previously described [76]. Briefly, the Dual-
715 Luciferase Reporter Assay System (Promega) was used in combination with the Veritas
716 Microplate Luminometer from Turner Biosystems to quantify activity of the two
717 luciferases. Frameshifting was calculated by first determining the ratio of firefly to renilla
718 luciferase activity for each sample, and then normalizing each out-of-frame construct
719 (pCWR43 and pCWR45) with their associated in-frame control (pCWR42 and pCWR44,
720 respectively).

721
722 **Proteomics.** UTI89, UTI89 Δ *miaA*, UTI89/pRR48, and UTI89/pMiaA_{P_{tac}} were grown to
723 mid-log phase (OD₆₀₀~0.5) in LB shaking at 37°C. IPTG (1 mM) was included for
724 UTI89/pRR48 and UTI89/pMiaA_{P_{tac}}. About 1X10⁹ CFU from each culture was pelleted at
725 8,000 x g for 1.5 minutes. Supernatants were then removed and cells were plunged into
726 liquid nitrogen and subsequently analyzed using MudPIT with the MSRC Proteomics Core
727 at Vanderbilt University. Label-free quantification (LFQ) values were loaded into Prostar

728 software for statistical analysis and visualization. The data set was filtered by requiring all
729 conditions to contain at least two values. Imputation for partially observed values was
730 done with the Structured Least Square Adaptive algorithm. Imputation for conditions in
731 which values were missing for a specific protein in all three biological replicates used the
732 DetQuantile algorithm with the settings Quantile:2.5 and Factor:1. Statistical analysis was
733 performed using the 1vs1 settings and Student's *t*-tests. Differentially expressed proteins
734 were categorized (**Supplemental Dataset S1**) based on literature searches and
735 information drawn from EcoCyc ([105]; <http://ecocyc.org/>), STRING Protein-Protein
736 Interaction Networks Functional Enrichment Analysis ([106]; <https://string-db.org/>), and
737 Phyre2 ([107]; <http://www.sbg.bio.ic.ac.uk/~phyre2/html/page.cgi?id=index>). The
738 proteomics output files will be uploaded to ProteomeXchange.

739

740 **RT-qPCR analysis.** UTI89 was diluted 1:100 from overnight cultures into fresh LB, grown
741 shaking for 2.5 hours at 37°C prior to resuspension in LB or LB + 5% NaCl. After another
742 one-hour incubation bacteria were pelleted and total RNA was extracted using the
743 miRNeasy mini kit (QIAGEN). RNA samples were treated with RNase-Free DNase
744 (QIAGEN) and cDNA was made using SuperScript IV VILO Master Mix (Invitrogen)
745 according to the manufacturer's protocol. Quantitative PCR (qPCR) was carried out using
746 primers listed in **Supplemental Table S2** with the PowerUp SYBR Green Master Mix
747 (Thermo Fisher Scientific) on a QuantStudio 3 Real-Time PCR Instrument (Applied
748 Biosystems). Replicas were made for each cDNA sample and *miaA* and *miaB* levels
749 were normalized to *rpoD*. Products were resolved in 1.5% agarose gels, stained with

750 ethidium bromide, and visualized using a GelDoc system (BioRad Technologies) to help
751 verify the specificity of the RT-qPCR results.

752

753 **Codon usage analysis.** Codon frequencies (UNN Stats tab, **Supplemental Dataset S1**)
754 were calculated for each gene in UTI89 (accessions CP000243.1 and CP000244.1) using
755 custom Python scripts that leverage the BioPython and NumPy packages.

756

757 **Statistical analysis.** *P* values were determined as indicated by Log-Rank (Mantel-Cox),
758 Mann-Whitney U tests, ANOVA, or Student's *t*-tests performed using Prism 9.0.0
759 software, with corrections as indicated (GraphPad Software). Data distribution normality
760 (Gaussian) was not assumed, such that non-parametric tests were used for the mouse
761 experiments. *P*-values of less than or equal to 0.05 were defined as significant.

762

763 **ACKNOWLEDGEMENTS**

764 We thank W. Hayes McDonald of the Vanderbilt School of Medicine Mass Spectrometry
765 Research Center for help with the proteomics. This study was funded in part by NIH grants
766 to M.A.M. (GM134331, AI135918, AI095647, and AI088086) and to V.B. (GM126956).
767 M.G.B. was supported by T32 AI055434 from the National Institute of Allergy and
768 Infectious Diseases, and A.J.L. was supported by T32 DK007115 from the National
769 Institute of Diabetes and Digestive and Kidney Diseases. The authors have no conflicts
770 of interest to declare.

771

772

773 **Author Contributions**

774 MGB, BAF, and MAM designed, supervised the study, performed research, analyzed the
775 data, and drafted the paper. WMK, AJL, JRB, MH, VB, and MTH helped with design,
776 experimentation, and editing. AT, CJB, LMB, and QZ performed experiments and helped
777 process samples. All authors contributed to and approved the submission of this paper.

778

779 **REFERENCES**

- 780 1. Jackman JE, Alfonzo JD. Transfer RNA modifications: nature's combinatorial
781 chemistry playground. *Wiley Interdiscip Rev RNA*. 2013;4(1):35-48. doi:
782 10.1002/wrna.1144. PubMed PMID: 23139145; PubMed Central PMCID:
783 PMCPMC3680101.
- 784 2. Bjork GR, Durand JM, Hagervall TG, Leipuviene R, Lundgren HK, Nilsson K, et
785 al. Transfer RNA modification: influence on translational frameshifting and metabolism.
786 *FEBS Lett*. 1999;452(1-2):47-51. Epub 1999/06/22. PubMed PMID: 10376676.
- 787 3. Gustilo EM, Vendeix FA, Agris PF. tRNA's modifications bring order to gene
788 expression. *Curr Opin Microbiol*. 2008;11(2):134-40. doi: 10.1016/j.mib.2008.02.003.
789 PubMed PMID: 18378185; PubMed Central PMCID: PMCPMC2408636.
- 790 4. Boccaletto P, Machnicka MA, Purta E, Piatkowski P, Baginski B, Wirecki TK, et
791 al. MODOMICS: a database of RNA modification pathways. 2017 update. *Nucleic Acids*
792 *Research*. 2018;46(D1):D303-d7. Epub 2017/11/07. doi: 10.1093/nar/gkx1030. PubMed
793 PMID: 29106616; PubMed Central PMCID: PMCPMC5753262.
- 794 5. Bjork GR, Hagervall TG. Transfer RNA Modification: Presence, Synthesis, and
795 Function. *EcoSal Plus*. 2014;6(1). doi: 10.1128/ecosalplus.ESP-0007-2013. PubMed
796 PMID: 26442937.
- 797 6. Blum PH. Reduced leu operon expression in a *miaA* mutant of *Salmonella*
798 *typhimurium*. *J Bacteriol*. 1988;170(11):5125-33. Epub 1988/11/01. PubMed PMID:
799 3141379; PubMed Central PMCID: PMC211580.
- 800 7. Thompson KM, Gottesman S. The MiaA tRNA modification enzyme is necessary
801 for robust RpoS expression in *Escherichia coli*. *J Bacteriol*. 2014;196(4):754-61. doi:

- 802 10.1128/JB.01013-13. PubMed PMID: 24296670; PubMed Central PMCID:
803 PMCPMC3911166.
- 804 8. Schweizer U, Bohleber S, Fradejas-Villar N. The modified base
805 isopentenyladenosine and its derivatives in tRNA. *RNA biology*. 2017;14(9):1197-208.
806 Epub 2017/03/10. doi: 10.1080/15476286.2017.1294309. PubMed PMID: 28277934;
807 PubMed Central PMCID: PMCPMC5699536.
- 808 9. Ahn KS, Ha U, Jia J, Wu D, Jin S. The *truA* gene of *Pseudomonas aeruginosa* is
809 required for the expression of type III secretory genes. *Microbiology*. 2004;150(Pt
810 3):539-47. Epub 2004/03/03. PubMed PMID: 14993303.
- 811 10. Shippy DC, Fadi AA. tRNA modification enzymes GidA and MnmE: potential role
812 in virulence of bacterial pathogens. *Int J Mol Sci*. 2014;15(10):18267-80. doi:
813 10.3390/ijms151018267. PubMed PMID: 25310651; PubMed Central PMCID:
814 PMCPMC4227215.
- 815 11. Durand JM, Dagberg B, Uhlin BE, Bjork GR. Transfer RNA modification,
816 temperature and DNA superhelicity have a common target in the regulatory network of
817 the virulence of *Shigella flexneri*: the expression of the *virF* gene. *Mol Microbiol*.
818 2000;35(4):924-35. Epub 2000/02/26. PubMed PMID: 10692168.
- 819 12. Chaudhuri RR, Peters SE, Pleasance SJ, Northen H, Willers C, Paterson GK, et
820 al. Comprehensive identification of *Salmonella enterica* serovar Typhimurium genes
821 required for infection of BALB/c mice. *PLoS Pathog*. 2009;5(7):e1000529. doi:
822 10.1371/journal.ppat.1000529. PubMed PMID: 19649318; PubMed Central PMCID:
823 PMCPMC2712085.
- 824 13. Gray J, Wang J, Gelvin SB. Mutation of the *miaA* gene of *Agrobacterium*
825 *tumefaciens* results in reduced *vir* gene expression. *J Bacteriol*. 1992;174(4):1086-98.
826 Epub 1992/02/01. PubMed PMID: 1735704; PubMed Central PMCID: PMC206401.
- 827 14. Chionh YH, McBee M, Babu IR, Hia F, Lin W, Zhao W, et al. tRNA-mediated
828 codon-biased translation in mycobacterial hypoxic persistence. *Nature Comm*.
829 2016;7:13302. Epub 2016/11/12. doi: 10.1038/ncomms13302. PubMed PMID:
830 27834374; PubMed Central PMCID: PMCPMC5114619.
- 831 15. Koshla O, Yushchuk O, Ostash I, Dacyuk Y, Myronovskyi M, Jager G, et al.
832 Gene *miaA* for post-transcriptional modification of tRNAXXA is important for

- 833 morphological and metabolic differentiation in *Streptomyces*. *Mol Microbiol.*
834 2019;112(1):249-65. Epub 2019/04/25. doi: 10.1111/mmi.14266. PubMed PMID:
835 31017319.
- 836 16. Thongdee N, Jaroensuk J, Atichartpongkul S, Chittrakanwong J, Chooyoung K,
837 Srimahaeak T, et al. TrmB, a tRNA m7G46 methyltransferase, plays a role in hydrogen
838 peroxide resistance and positively modulates the translation of *katA* and *katB* mRNAs in
839 *Pseudomonas aeruginosa*. *Nucleic acids research.* 2019;47(17):9271-81. Epub
840 2019/08/21. doi: 10.1093/nar/gkz702. PubMed PMID: 31428787; PubMed Central
841 PMCID: PMCPMC6755087.
- 842 17. Gao T, Tan M, Liu W, Zhang C, Zhang T, Zheng L, et al. GidA, a tRNA
843 Modification Enzyme, Contributes to the Growth, and Virulence of *Streptococcus suis*
844 Serotype 2. *Front Cell Infect Microbiol.* 2016;6:44. Epub 2016/05/06. doi:
845 10.3389/fcimb.2016.00044. PubMed PMID: 27148493; PubMed Central PMCID:
846 PMCPMC4835480.
- 847 18. Li D, Shibata Y, Takeshita T, Yamashita Y. A novel gene involved in the survival
848 of *Streptococcus mutans* under stress conditions. *Applied and Environmental*
849 *Microbiology.* 2014;80(1):97-103. Epub 2013/10/15. doi: 10.1128/AEM.02549-13.
850 PubMed PMID: 24123744; PubMed Central PMCID: PMCPMC3910998.
- 851 19. Cho KH, Caparon MG. tRNA modification by GidA/MnmE is necessary for
852 *Streptococcus pyogenes* virulence: a new strategy to make live attenuated strains.
853 *Infection and Immunity.* 2008;76(7):3176-86. Epub 2008/04/23. doi: 10.1128/IAI.01721-
854 07. PubMed PMID: 18426891; PubMed Central PMCID: PMCPMC2446735.
- 855 20. Kinscherf TG, Willis DK. Global regulation by *gidA* in *Pseudomonas syringae*. *J*
856 *Bacteriol.* 2002;184(8):2281-6. Epub 2002/03/27. doi: 10.1128/jb.184.8.2281-
857 2286.2002. PubMed PMID: 11914360; PubMed Central PMCID: PMCPMC134964.
- 858 21. Sha J, Kozlova EV, Fadl AA, Olano JP, Houston CW, Peterson JW, et al.
859 Molecular characterization of a glucose-inhibited division gene, *gidA*, that regulates
860 cytotoxic enterotoxin of *Aeromonas hydrophila*. *Infection and immunity.*
861 2004;72(2):1084-95. Epub 2004/01/27. doi: 10.1128/iai.72.2.1084-1095.2004. PubMed
862 PMID: 14742556; PubMed Central PMCID: PMCPMC321642.

- 863 22. Kaminska KH, Baraniak U, Boniecki M, Nowaczyk K, Czerwoniec A, Bujnicki JM.
864 Structural bioinformatics analysis of enzymes involved in the biosynthesis pathway of
865 the hypermodified nucleoside ms(2)io(6)A37 in tRNA. *Proteins*. 2008;70(1):1-18. Epub
866 2007/10/03. doi: 10.1002/prot.21640. PubMed PMID: 17910062.
- 867 23. Persson BC. Modification of tRNA as a regulatory device. *Mol Microbiol*.
868 1993;8(6):1011-6. Epub 1993/06/01. PubMed PMID: 7689685.
- 869 24. Caillet J, Droogmans L. Molecular cloning of the *Escherichia coli miaA* gene
870 involved in the formation of delta 2-isopentenyl adenosine in tRNA. *J Bacteriol*.
871 1988;170(9):4147-52. Epub 1988/09/01. PubMed PMID: 3045085; PubMed Central
872 PMCID: PMC211421.
- 873 25. Seif E, Hallberg BM. RNA-protein mutually induced fit: structure of *Escherichia*
874 *coli* isopentenyl-tRNA transferase in complex with tRNA(Phe). *J Biol Chem*.
875 2009;284(11):6600-4. Epub 2009/01/23. doi: 10.1074/jbc.C800235200. PubMed PMID:
876 19158097; PubMed Central PMCID: PMC2652265.
- 877 26. Pierrel F, Douki T, Fontecave M, Atta M. MiaB protein is a bifunctional radical-S-
878 adenosylmethionine enzyme involved in thiolation and methylation of tRNA. *J Biol*
879 *Chem*. 2004;279(46):47555-63. Epub 2004/09/02. doi: 10.1074/jbc.M408562200.
880 PubMed PMID: 15339930.
- 881 27. Ericson JU, Bjork GR. Pleiotropic effects induced by modification deficiency next
882 to the anticodon of tRNA from *Salmonella typhimurium* LT2. *J Bacteriol*.
883 1986;166(3):1013-21. Epub 1986/06/01. PubMed PMID: 2423501; PubMed Central
884 PMCID: PMC215226.
- 885 28. Eisenberg SP, Yarus M, Soll L. The effect of an *Escherichia coli* regulatory
886 mutation on transfer RNA structure. *J Mol Biol*. 1979;135(1):111-26. PubMed PMID:
887 93644.
- 888 29. Gowrishankar J, Pittard J. Regulation of phenylalanine biosynthesis in
889 *Escherichia coli* K-12: control of transcription of the *pheA* operon. *J Bacteriol*.
890 1982;150(3):1130-7. PubMed PMID: 7042684; PubMed Central PMCID:
891 PMCPMC216333.
- 892 30. Aubee JI, Olu M, Thompson KM. TrmL and TusA Are Necessary for *rpoS* and
893 *MiaA* Is Required for *hfq* Expression in *Escherichia coli*. *Biomolecules*. 2017;7(2). Epub

- 894 2017/05/05. doi: 10.3390/biom7020039. PubMed PMID: 28471404; PubMed Central
895 PMCID: PMCPMC5485728.
- 896 31. Aubee JI, Olu M, Thompson KM. The i6A37 tRNA modification is essential for
897 proper decoding of UUX-Leucine codons during *rpoS* and *iraP* translation. RNA (New
898 York, NY). 2016;22(5):729-42. Epub 2016/03/17. doi: 10.1261/rna.053165.115. PubMed
899 PMID: 26979278; PubMed Central PMCID: PMCPMC4836647.
- 900 32. Krasich R, Wu SY, Kuo HK, Kreuzer KN. Functions that protect *Escherichia coli*
901 from DNA-protein crosslinks. DNA Repair (Amst). 2015;28:48-59. doi:
902 10.1016/j.dnarep.2015.01.016. PubMed PMID: 25731940; PubMed Central PMCID:
903 PMCPMC4385401.
- 904 33. Connolly DM, Winkler ME. Genetic and physiological relationships among the
905 *miaA* gene, 2-methylthio-N⁶-(delta 2-isopentenyl)-adenosine tRNA modification, and
906 spontaneous mutagenesis in *Escherichia coli* K-12. J Bacteriol. 1989;171(6):3233-46.
907 Epub 1989/06/01. PubMed PMID: 2656644; PubMed Central PMCID: PMC210042.
- 908 34. Yanofsky C. Mutations affecting tRNA^{Trp} and its charging and their effect on
909 regulation of transcription termination at the attenuator of the tryptophan operon.
910 Journal of Molecular Biology. 1977;113(4):663-77. Epub 1977/07/15. PubMed PMID:
911 330867.
- 912 35. Mikkola R, Kurlan CG. Media dependence of translational mutant phenotype.
913 FEMS Microbiol Lett 1988;56(3):265-9. doi: DOI: [http://dx.doi.org/10.1111/j.1574-
914 6968.1988.tb03189.x](http://dx.doi.org/10.1111/j.1574-6968.1988.tb03189.x).
- 915 36. Forouhar F, Arragain S, Atta M, Gambarelli S, Mouesca JM, Hussain M, et al.
916 Two Fe-S clusters catalyze sulfur insertion by radical-SAM methylthiotransferases. Nat
917 Chem Biol. 2013;9(5):333-8. doi: 10.1038/nchembio.1229. PubMed PMID: 23542644;
918 PubMed Central PMCID: PMCPMC4118475.
- 919 37. Leung HC, Chen Y, Winkler ME. Regulation of substrate recognition by the MiaA
920 tRNA prenyltransferase modification enzyme of *Escherichia coli* K-12. J Biol Chem.
921 1997;272(20):13073-83. Epub 1997/05/16. PubMed PMID: 9148919.
- 922 38. Denamur E, Clermont O, Bonacorsi S, Gordon D. The population genetics of
923 pathogenic *Escherichia coli*. Nat Rev Microbiol. 2021;19(1):37-54. Epub 2020/08/23.
924 doi: 10.1038/s41579-020-0416-x. PubMed PMID: 32826992.

- 925 39. Vila J, Saez-Lopez E, Johnson JR, Romling U, Dobrindt U, Canton R, et al.
926 *Escherichia coli*: an old friend with new tidings. FEMS microbiology reviews.
927 2016;40(4):437-63. Epub 2017/02/16. doi: 10.1093/femsre/fuw005. PubMed PMID:
928 28201713.
- 929 40. Barber AE, Norton JP, Spivak AM, Mulvey MA. Urinary tract infections: current
930 and emerging management strategies. Clin Infect Dis. 2013;57(5):719-24. Epub
931 2013/05/07. doi: 10.1093/cid/cit284. PubMed PMID: 23645845; PubMed Central
932 PMCID: PMC3739462.
- 933 41. Hunstad DA, Justice SS. Intracellular lifestyles and immune evasion strategies of
934 uropathogenic *Escherichia coli*. Annu Rev Microbiol. 2010;64:203-21. Epub 2010/09/10.
935 doi: 10.1146/annurev.micro.112408.134258. PubMed PMID: 20825346.
- 936 42. Schwab S, Jobin K, Kurts C. Urinary tract infection: recent insight into the
937 evolutionary arms race between uropathogenic *Escherichia coli* and our immune
938 system. Nephrology, Dialysis, Transplantation: official publication of the European
939 Dialysis and Transplant Association - European Renal Association. 2017;32(12):1977-
940 83. Epub 2017/03/25. doi: 10.1093/ndt/gfx022. PubMed PMID: 28340252.
- 941 43. O'Brien VP, Hannan TJ, Schaeffer AJ, Hultgren SJ. Are you experienced?
942 Understanding bladder innate immunity in the context of recurrent urinary tract infection.
943 Curr Opin Infect Dis. 2015;28(1):97-105. doi: 10.1097/QCO.000000000000130.
944 PubMed PMID: 25517222; PubMed Central PMCID: PMC3739462.
- 945 44. Lacerda Mariano L, Ingersoll MA. The immune response to infection in the
946 bladder. Nat Rev Urol. 2020;17(8):439-58. Epub 2020/07/15. doi: 10.1038/s41585-020-
947 0350-8. PubMed PMID: 32661333.
- 948 45. Svensson L, Poljakovic M, Demirel I, Sahlberg C, Persson K. Host-Derived Nitric
949 Oxide and Its Antibacterial Effects in the Urinary Tract. Adv Microb Physiol. 2018;73:1-
950 62. Epub 2018/09/29. doi: 10.1016/bs.ampbs.2018.05.001. PubMed PMID: 30262107.
- 951 46. Chan CT, Dyavaiah M, DeMott MS, Taghizadeh K, Dedon PC, Begley TJ. A
952 quantitative systems approach reveals dynamic control of tRNA modifications during
953 cellular stress. PLoS Genet. 2010;6(12):e1001247. Epub 2010/12/29. doi:
954 10.1371/journal.pgen.1001247. PubMed PMID: 21187895; PubMed Central PMCID:
955 PMC3002981.

- 956 47. Barber AE, Norton JP, Wiles TJ, Mulvey MA. Strengths and Limitations of Model
957 Systems for the Study of Urinary Tract Infections and Related Pathologies. *Microbiology*
958 and *Molecular Biology Reviews*: MMBR. 2016;80(2):351-67. Epub 2016/03/05. doi:
959 10.1128/MMBR.00067-15. PubMed PMID: 26935136; PubMed Central PMCID:
960 PMCPMC4867371.
- 961 48. Datsenko KA, Wanner BL. One-step inactivation of chromosomal genes in
962 *Escherichia coli* K-12 using PCR products. *Proc Natl Acad Sci U S A*.
963 2000;97(12):6640-5. PubMed PMID: 10829079.
- 964 49. Murphy KC, Campellone KG. Lambda Red-mediated recombinogenic
965 engineering of enterohemorrhagic and enteropathogenic *E. coli*. *BMC Mol Biol*.
966 2003;4:11. PubMed PMID: 14672541.
- 967 50. Forde BM, Roberts LW, Phan MD, Peters KM, Fleming BA, Russell CW, et al.
968 Population dynamics of an *Escherichia coli* ST131 lineage during recurrent urinary tract
969 infection. *Nature Comm*. 2019;10(1):3643. Epub 2019/08/15. doi: 10.1038/s41467-019-
970 11571-5. PubMed PMID: 31409795; PubMed Central PMCID: PMC6692316.
- 971 51. Moreno E, Andreu A, Pigrau C, Kuskowski MA, Johnson JR, Prats G.
972 Relationship between *Escherichia coli* strains causing acute cystitis in women and the
973 fecal *E. coli* population of the host. *Journal of Clinical Microbiology*. 2008;46(8):2529-34.
974 Epub 2008/05/23. doi: 10.1128/jcm.00813-08. PubMed PMID: 18495863; PubMed
975 Central PMCID: PMC6692316.
- 976 52. Chen SL, Wu M, Henderson JP, Hooton TM, Hibbing ME, Hultgren SJ, et al.
977 Genomic diversity and fitness of *E. coli* strains recovered from the intestinal and urinary
978 tracts of women with recurrent urinary tract infection. *Science Translational Medicine*.
979 2013;5(184):184ra60. doi: 10.1126/scitranslmed.3005497. PubMed PMID: 23658245;
980 PubMed Central PMCID: PMC3695744.
- 981 53. Yamamoto S, Tsukamoto T, Terai A, Kurazono H, Takeda Y, Yoshida O. Genetic
982 evidence supporting the fecal-perineal-urethral hypothesis in cystitis caused by
983 *Escherichia coli*. *J Urol*. 1997;157(3):1127-9. PubMed PMID: 9072556.
- 984 54. Russo TA, Stapleton A, Wenderoth S, Hooton TM, Stamm WE. Chromosomal
985 restriction fragment length polymorphism analysis of *Escherichia coli* strains causing

- 986 recurrent urinary tract infections in young women. *J Infect Dis.* 1995;172(2):440-5. Epub
987 1995/08/01. doi: 10.1093/infdis/172.2.440. PubMed PMID: 7622887.
- 988 55. Russell CW, Fleming BA, Jost CA, Tran A, Stenquist AT, Wambaugh MA, et al.
989 Context-Dependent Requirements for FimH and Other Canonical Virulence Factors in
990 Gut Colonization by Extraintestinal Pathogenic *Escherichia coli*. *Infection and Immunity.*
991 2018;86(3). Epub 2018/01/10. doi: 10.1128/IAI.00746-17. PubMed PMID: 29311232;
992 PubMed Central PMCID: PMC5820936.
- 993 56. Russell CW, Mulvey MA. The Extraintestinal Pathogenic *Escherichia coli* Factor
994 RqII Constrains the Genotoxic Effects of the RecQ-Like Helicase RqIH. *PLoS Pathog.*
995 2015;11(12):e1005317. doi: 10.1371/journal.ppat.1005317. PubMed PMID: 26636713;
996 PubMed Central PMCID: PMC4670107.
- 997 57. Russell CW, Richards AC, Chang AS, Mulvey MA. The Rhomboid Protease
998 GlpG Promotes the Persistence of Extraintestinal Pathogenic *Escherichia coli* within the
999 Gut. *Infection and Immunity.* 2017;85(6). Epub 2017/04/05. doi: 10.1128/IAI.00866-16.
1000 PubMed PMID: 28373355; PubMed Central PMCID: PMC5442614.
- 1001 58. Lewis AJ, Richards AC, Mulvey MA. Invasion of Host Cells and Tissues by
1002 Uropathogenic Bacteria. *Microbiol Spectr.* 2016;4(6). Epub 2017/01/15. doi:
1003 10.1128/microbiolspec.UTI-0026-2016. PubMed PMID: 28087946; PubMed Central
1004 PMCID: PMC5244466.
- 1005 59. Hagberg L, Hull R, Hull S, McGhee JR, Michalek SM, Svanborg Eden C.
1006 Difference in susceptibility to gram-negative urinary tract infection between C3H/HeJ
1007 and C3H/HeN mice. *Infection and Immunity.* 1984;46(3):839-44.
- 1008 60. Suhs KA, Marthaler BR, Welch RA, Hopkins WJ. Lack of association between
1009 the Tlr4 (Lpsd/Lpsd) genotype and increased susceptibility to *Escherichia coli* bladder
1010 infections in female C3H/HeJ mice. *MBio.* 2011;2(3):e00094-11. Epub 2011/06/02. doi:
1011 10.1128/mBio.00094-11 e00094-11 [pii] mBio.00094-11 [pii]. PubMed PMID: 21628500;
1012 PubMed Central PMCID: PMC3104495.
- 1013 61. Hopkins WJ, Elkahwaji J, Kendzioriski C, Moser AR, Briggs PM, Suhs KA.
1014 Quantitative trait loci associated with susceptibility to bladder and kidney infections
1015 induced by *Escherichia coli* in female C3H/HeJ mice. *J Infect Dis.* 2009;199(3):355-61.

- 1016 Epub 2008/12/09. doi: 10.1086/595987. PubMed PMID: 19061424; PubMed Central
1017 PMCID: PMC2683358.
- 1018 62. Donovan GT, Norton JP, Bower JM, Mulvey MA. Adenylate cyclase and the
1019 cyclic AMP receptor protein modulate stress resistance and virulence capacity of
1020 uropathogenic *Escherichia coli*. Infection and Immunity. 2013;81(1):249-58. Epub
1021 2012/11/02. doi: 10.1128/iai.00796-12. PubMed PMID: 23115037; PubMed Central
1022 PMCID: PMCPMC3536135.
- 1023 63. van der Mee-Marquet NL, Blanc DS, Gbaguidi-Haore H, Dos Santos Borges S,
1024 Viboud Q, Bertrand X, et al. Marked increase in incidence for bloodstream infections
1025 due to *Escherichia coli*, a side effect of previous antibiotic therapy in the elderly. Front
1026 Microbiol. 2015;6:646. doi: 10.3389/fmicb.2015.00646. PubMed PMID: 26175721.
- 1027 64. Picard B, Garcia JS, Gouriou S, Duriez P, Brahim N, Bingen E, et al. The link
1028 between phylogeny and virulence in *Escherichia coli* extraintestinal infection. Infection
1029 and immunity. 1999;67(2):546-53. Epub 1999/01/23. doi: 10.1128/IAI.67.2.546-
1030 553.1999. PubMed PMID: 9916057; PubMed Central PMCID: PMCPMC96353.
- 1031 65. Trivedi S, Labuz D, Anderson CP, Araujo CV, Blair A, Middleton EA, et al.
1032 Mucosal-associated invariant T (MAIT) cells mediate protective host responses in
1033 sepsis. Elife. 2020;9. Epub 2020/11/10. doi: 10.7554/eLife.55615. PubMed PMID:
1034 33164745; PubMed Central PMCID: PMCPMC7679140.
- 1035 66. Mikkola R, Kurland CG. Evidence for demand-regulation of ribosome
1036 accumulation in *E. coli*. Biochimie. 1991;73(12):1551-6. Epub 1991/12/01. PubMed
1037 PMID: 1805968.
- 1038 67. Korshunov S, Imlay JA. Detection and quantification of superoxide formed within
1039 the periplasm of *Escherichia coli*. J Bacteriol. 2006;188(17):6326-34. PubMed PMID:
1040 16923900.
- 1041 68. Bower JM, Mulvey MA. Polyamine-mediated resistance of uropathogenic
1042 *Escherichia coli* to nitrosative stress. J Bacteriol. 2006;188(3):928-33. Epub 2006/01/24.
1043 doi: 188/3/928 [pii] 10.1128/JB.188.3.928-933.2006. PubMed PMID: 16428396.
- 1044 69. Woolford G, Casselden RJ, Walters CL. Gaseous products of the interaction of
1045 sodium nitrite with porcine skeletal muscle. Biochem J. 1972;130(2):82P-3P. Epub

- 1046 1972/11/01. doi: 10.1042/bj1300082pb. PubMed PMID: 4664608; PubMed Central
1047 PMCID: PMCPMC1174485.
- 1048 70. Hassan HM, Fridovich I. Superoxide radical and the oxygen enhancement of the
1049 toxicity of paraquat in *Escherichia coli*. J Biol Chem. 1978;253(22):8143-8. Epub
1050 1978/11/25. PubMed PMID: 213429.
- 1051 71. Withman B, Gunasekera TS, Beesetty P, Agans R, Paliy O. Transcriptional
1052 responses of uropathogenic *Escherichia coli* to increased environmental osmolality
1053 caused by salt or urea. Infection and immunity. 2013;81(1):80-9. Epub 2012/10/24. doi:
1054 10.1128/iai.01049-12. PubMed PMID: 23090957; PubMed Central PMCID:
1055 PMCPMC3536127.
- 1056 72. Schwan WR. Survival of uropathogenic *Escherichia coli* in the murine urinary
1057 tract is dependent on OmpR. Microbiology. 2009;155(Pt 6):1832-9. Epub 2009/04/23.
1058 doi: mic.0.026187-0 [pii]
1059 10.1099/mic.0.026187-0. PubMed PMID: 19383700.
- 1060 73. Urbonavicius J, Qian Q, Durand JM, Hagervall TG, Bjork GR. Improvement of
1061 reading frame maintenance is a common function for several tRNA modifications.
1062 EMBO J. 2001;20(17):4863-73. Epub 2001/09/05. doi: 10.1093/emboj/20.17.4863.
1063 PubMed PMID: 11532950; PubMed Central PMCID: PMC125605.
- 1064 74. Urbonavicius J, Stahl G, Durand JM, Ben Salem SN, Qian Q, Farabaugh PJ, et
1065 al. Transfer RNA modifications that alter +1 frameshifting in general fail to affect -1
1066 frameshifting. RNA (New York, NY). 2003;9(6):760-8. Epub 2003/05/21. PubMed PMID:
1067 12756333; PubMed Central PMCID: PMC1370442.
- 1068 75. Howard MT, Shirts BH, Zhou J, Carlson CL, Matsufuji S, Gesteland RF, et al.
1069 Cell culture analysis of the regulatory frameshift event required for the expression of
1070 mammalian antizymes. Genes to Cells. 2001;6(11):931-41. Epub 2001/12/26. PubMed
1071 PMID: 11733031.
- 1072 76. Grentzmann G, Ingram JA, Kelly PJ, Gesteland RF, Atkins JF. A dual-luciferase
1073 reporter system for studying recoding signals. RNA (New York, NY). 1998;4(4):479-86.
1074 Epub 1998/06/18. PubMed PMID: 9630253; PubMed Central PMCID:
1075 PMCPMC1369633.

- 1076 77. Floyd KA, Moore JL, Eberly AR, Good JA, Shaffer CL, Zaver H, et al. Adhesive
1077 fiber stratification in uropathogenic *Escherichia coli* biofilms unveils oxygen-mediated
1078 control of type 1 pili. PLoS Pathog. 2015;11(3):e1004697. Epub 2015/03/05. doi:
1079 10.1371/journal.ppat.1004697. PubMed PMID: 25738819; PubMed Central PMCID:
1080 PMCPMC4349694.
- 1081 78. Beebout CJ, Eberly AR, Werby SH, Reasoner SA, Brannon JR, De S, et al.
1082 Respiratory Heterogeneity Shapes Biofilm Formation and Host Colonization in
1083 Uropathogenic *Escherichia coli*. MBio. 2019;10(2). Epub 2019/04/04. doi:
1084 10.1128/mBio.02400-18. PubMed PMID: 30940709; PubMed Central PMCID:
1085 PMCPMC6445943.
- 1086 79. Wolf J, Gerber AP, Keller W. tadA, an essential tRNA-specific adenosine
1087 deaminase from *Escherichia coli*. EMBO J. 2002;21(14):3841-51. Epub 2002/07/12. doi:
1088 10.1093/emboj/cdf362. PubMed PMID: 12110595; PubMed Central PMCID:
1089 PMCPMC126108.
- 1090 80. Bar-Yaacov D, Mordret E, Towers R, Biniashvili T, Soyris C, Schwartz S, et al.
1091 RNA editing in bacteria recodes multiple proteins and regulates an evolutionarily
1092 conserved toxin-antitoxin system. Genome Res. 2017;27(10):1696-703. Epub
1093 2017/09/03. doi: 10.1101/gr.222760.117. PubMed PMID: 28864459; PubMed Central
1094 PMCID: PMCPMC5630033.
- 1095 81. Kulesus RR, Diaz-Perez K, Slechta ES, Eto DS, Mulvey MA. Impact of the RNA
1096 chaperone Hfq on the fitness and virulence potential of uropathogenic *Escherichia coli*.
1097 Infection and Immunity. 2008;76(7):3019-26. Epub 2008/05/07. doi: IAI.00022-08 [pii]
1098 10.1128/IAI.00022-08. PubMed PMID: 18458066.
- 1099 82. Endres L, Dedon PC, Begley TJ. Codon-biased translation can be regulated by
1100 wobble-base tRNA modification systems during cellular stress responses. RNA biology.
1101 2015;12(6):603-14. Epub 2015/04/22. doi: 10.1080/15476286.2015.1031947. PubMed
1102 PMID: 25892531; PubMed Central PMCID: PMCPMC4615639.
- 1103 83. Koh CS, Sarin LP. Transfer RNA modification and infection - Implications for
1104 pathogenicity and host responses. Biochim Biophys Acta Gene Regul Mech.
1105 2018;1861(4):419-32. Epub 2018/01/30. doi: 10.1016/j.bbagr.2018.01.015. PubMed
1106 PMID: 29378328.

- 1107 84. Durand JM, Bjork GR, Kuwae A, Yoshikawa M, Sasakawa C. The modified
1108 nucleoside 2-methylthio-N6-isopentenyladenosine in tRNA of *Shigella flexneri* is
1109 required for expression of virulence genes. J Bacteriol. 1997;179(18):5777-82. Epub
1110 1997/09/19. doi: 10.1128/jb.179.18.5777-5782.1997. PubMed PMID: 9294434; PubMed
1111 Central PMCID: PMCPMC179466.
- 1112 85. Tsui HC, Winkler ME. Transcriptional patterns of the mutL-miaA superoperon of
1113 *Escherichia coli* K-12 suggest a model for posttranscriptional regulation. Biochimie.
1114 1994;76(12):1168-77. Epub 1994/01/01. doi: 10.1016/0300-9084(94)90046-9. PubMed
1115 PMID: 7748952.
- 1116 86. Connolly DM, Winkler ME. Structure of *Escherichia coli* K-12 miaA and
1117 characterization of the mutator phenotype caused by *miaA* insertion mutations. J
1118 Bacteriol. 1991;173(5):1711-21. Epub 1991/03/01. doi: 10.1128/jb.173.5.1711-
1119 1721.1991. PubMed PMID: 1999389; PubMed Central PMCID: PMCPMC207322.
- 1120 87. Dedon PC, Begley TJ. A system of RNA modifications and biased codon use
1121 controls cellular stress response at the level of translation. Chemical Research in
1122 Toxicology. 2014;27(3):330-7. Epub 2014/01/16. doi: 10.1021/tx400438d. PubMed
1123 PMID: 24422464; PubMed Central PMCID: PMCPMC3997223.
- 1124 88. Chan CT, Pang YL, Deng W, Babu IR, Dyavaiah M, Begley TJ, et al.
1125 Reprogramming of tRNA modifications controls the oxidative stress response by codon-
1126 biased translation of proteins. Nature Comm. 2012;3:937. Epub 2012/07/05. doi:
1127 10.1038/ncomms1938. PubMed PMID: 22760636; PubMed Central PMCID:
1128 PMCPMC3535174.
- 1129 89. Rehl JM, Shippy DC, Eakley NM, Brevik MD, Sand JM, Cook ME, et al. GidA
1130 expression in *Salmonella* is modulated under certain environmental conditions. Curr
1131 Microbiol. 2013;67(3):279-85. Epub 2013/04/13. doi: 10.1007/s00284-013-0361-2.
1132 PubMed PMID: 23579313.
- 1133 90. Pollo-Oliveira L, de Crecy-Lagard V. Can Protein Expression Be Regulated by
1134 Modulation of tRNA Modification Profiles? Biochemistry. 2019;58(5):355-62. Epub
1135 2018/12/05. doi: 10.1021/acs.biochem.8b01035. PubMed PMID: 30511849; PubMed
1136 Central PMCID: PMCPMC6363828.

- 1137 91. Wong GT, Bonocora RP, Schep AN, Beeler SM, Lee Fong AJ, Shull LM, et al.
1138 Genome-Wide Transcriptional Response to Varying RpoS Levels in *Escherichia coli* K-
1139 12. J Bacteriol. 2017;199(7). Epub 2017/01/25. doi: 10.1128/JB.00755-16. PubMed
1140 PMID: 28115545; PubMed Central PMCID: PMC5350281.
- 1141 92. Battesti A, Majdalani N, Gottesman S. The RpoS-mediated general stress
1142 response in *Escherichia coli*. Annu Rev Microbiol. 2011;65:189-213. Epub 2011/06/07.
1143 doi: 10.1146/annurev-micro-090110-102946. PubMed PMID: 21639793.
- 1144 93. Chao Y, Papenfort K, Reinhardt R, Sharma CM, Vogel J. An atlas of Hfq-bound
1145 transcripts reveals 3' UTRs as a genomic reservoir of regulatory small RNAs. EMBO J.
1146 2012;31(20):4005-19. Epub 2012/08/28. doi: 10.1038/emboj.2012.229. PubMed PMID:
1147 22922465; PubMed Central PMCID: PMC3474919.
- 1148 94. Pan T. Adaptive translation as a mechanism of stress response and adaptation.
1149 Annual Review of Genetics. 2013;47:121-37. Epub 2013/08/31. doi: 10.1146/annurev-
1150 genet-111212-133522. PubMed PMID: 23988117; PubMed Central PMCID:
1151 PMC4109725.
- 1152 95. Drummond DA, Wilke CO. The evolutionary consequences of erroneous protein
1153 synthesis. Nat Rev Genet. 2009;10(10):715-24. doi: 10.1038/nrg2662. PubMed PMID:
1154 19763154; PubMed Central PMCID: PMC2764353.
- 1155 96. Moura GR, Carreto LC, Santos MA. Genetic code ambiguity: an unexpected
1156 source of proteome innovation and phenotypic diversity. Curr Opin Microbiol.
1157 2009;12(6):631-7. doi: 10.1016/j.mib.2009.09.004. PubMed PMID: 19853500.
- 1158 97. Mohler K, Ibba M. Translational fidelity and mistranslation in the cellular response
1159 to stress. Nature Microbiology. 2017;2:17117. Epub 2017/08/25. doi:
1160 10.1038/nmicrobiol.2017.117. PubMed PMID: 28836574; PubMed Central PMCID:
1161 PMC5697424.
- 1162 98. Blango MG, Mulvey MA. Persistence of uropathogenic *Escherichia coli* in the
1163 face of multiple antibiotics. Antimicrob Agents Chemother. 2010;54(5):1855-63. Epub
1164 2010/03/17. doi: AAC.00014-10 [pii] 10.1128/AAC.00014-10. PubMed PMID: 20231390;
1165 PubMed Central PMCID: PMC2863638.
- 1166 99. Mulvey MA, Lopez-Boado YS, Wilson CL, Roth R, Parks WC, Heuser J, et al.
1167 Induction and evasion of host defenses by type 1-piliated uropathogenic *Escherichia*

- 1168 *coli*. Science (New York, NY). 1998;282(5393):1494-7. Epub 1998/11/20. PubMed
1169 PMID: 9822381.
- 1170 100. Blango MG, Ott EM, Erman A, Veranic P, Mulvey MA. Forced resurgence and
1171 targeting of intracellular uropathogenic *Escherichia coli* reservoirs. PloS One.
1172 2014;9(3):e93327. Epub 2014/03/29. doi: 10.1371/journal.pone.0093327. PubMed
1173 PMID: 24667805; PubMed Central PMCID: PMC3965547.
- 1174 101. Parkinson JS. cheA, cheB, and cheC genes of *Escherichia coli* and their role in
1175 chemotaxis. J Bacteriol. 1976;126(2):758-70. Epub 1976/05/01. doi:
1176 10.1128/JB.126.2.758-770.1976. PubMed PMID: 770453; PubMed Central PMCID:
1177 PMCPMC233211.
- 1178 102. Eto DS, Gordon HB, Dhakal BK, Jones TA, Mulvey MA. Clathrin, AP-2, and the
1179 NPXY-binding subset of alternate endocytic adaptors facilitate FimH-mediated bacterial
1180 invasion of host cells. Cellular Microbiology. 2008;10(12):2553-67. Epub 2008/08/30.
1181 doi: 10.1111/j.1462-5822.2008.01229.x. PubMed PMID: 18754852.
- 1182 103. Miles ZD, Myers WK, Kincannon WM, Britt RD, Bandarian V. Biochemical and
1183 Spectroscopic Studies of Epoxyqueuosine Reductase: A Novel Iron-Sulfur Cluster- and
1184 Cobalamin-Containing Protein Involved in the Biosynthesis of Queuosine. Biochemistry.
1185 2015;54(31):4927-35. Epub 2015/08/01. doi: 10.1021/acs.biochem.5b00335. PubMed
1186 PMID: 26230193; PubMed Central PMCID: PMCPMC4753064.
- 1187 104. Miles ZD, McCarty RM, Molnar G, Bandarian V. Discovery of epoxyqueuosine
1188 (oQ) reductase reveals parallels between halorespiration and tRNA modification. Proc
1189 Natl Acad Sci U S A. 2011;108(18):7368-72. Epub 2011/04/20. doi:
1190 10.1073/pnas.1018636108. PubMed PMID: 21502530; PubMed Central PMCID:
1191 PMCPMC3088584.
- 1192 105. Keseler IM, Mackie A, Santos-Zavaleta A, Billington R, Bonavides-Martinez C,
1193 Caspi R, et al. The EcoCyc database: reflecting new knowledge about *Escherichia coli*
1194 K-12. Nucleic acids research. 2017;45(D1):D543-D50. Epub 2016/12/03. doi:
1195 10.1093/nar/gkw1003. PubMed PMID: 27899573; PubMed Central PMCID:
1196 PMCPMC5210515.
- 1197 106. Szklarczyk D, Gable AL, Lyon D, Junge A, Wyder S, Huerta-Cepas J, et al.
1198 STRING v11: protein-protein association networks with increased coverage, supporting

1199 functional discovery in genome-wide experimental datasets. *Nucleic Acids Research*.
1200 2019;47(D1):D607-D13. Epub 2018/11/27. doi: 10.1093/nar/gky1131. PubMed PMID:
1201 30476243; PubMed Central PMCID: PMCPMC6323986.

1202 107. Kelley LA, Mezulis S, Yates CM, Wass MN, Sternberg MJ. The Phyre2 web
1203 portal for protein modeling, prediction and analysis. *Nat Protoc*. 2015;10(6):845-58.
1204 Epub 2015/05/08. doi: 10.1038/nprot.2015.053. PubMed PMID: 25950237; PubMed
1205 Central PMCID: PMCPMC5298202.

1206 108. Mulvey MA, Schilling JD, Hultgren SJ. Establishment of a persistent *Escherichia*
1207 *coli* reservoir during the acute phase of a bladder infection. *Infection and Immunity*.
1208 2001;69(7):4572-9. PubMed PMID: 11402001.

1209 109. Guzman LM, Belin D, Carson MJ, Beckwith J. Tight regulation, modulation, and
1210 high-level expression by vectors containing the arabinose PBAD promoter. *J Bacteriol*.
1211 1995;177(14):4121-30. Epub 1995/07/01. doi: 10.1128/jb.177.14.4121-4130.1995.
1212 PubMed PMID: 7608087; PubMed Central PMCID: PMCPMC177145.

1213 110. Zhou Q, Ames P, Parkinson JS. Mutational analyses of HAMP helices suggest a
1214 dynamic bundle model of input-output signalling in chemoreceptors. *Mol Microbiol*.
1215 2009;73(5):801-14. Epub 2009/08/07. doi: 10.1111/j.1365-2958.2009.06819.x. PubMed
1216 PMID: 19656294; PubMed Central PMCID: PMCPMC2749569.

1217

1218 **FIGURE LEGENDS**

1219 **Figure 1. MiaA promotes ExPEC fitness and virulence within diverse host niches.**

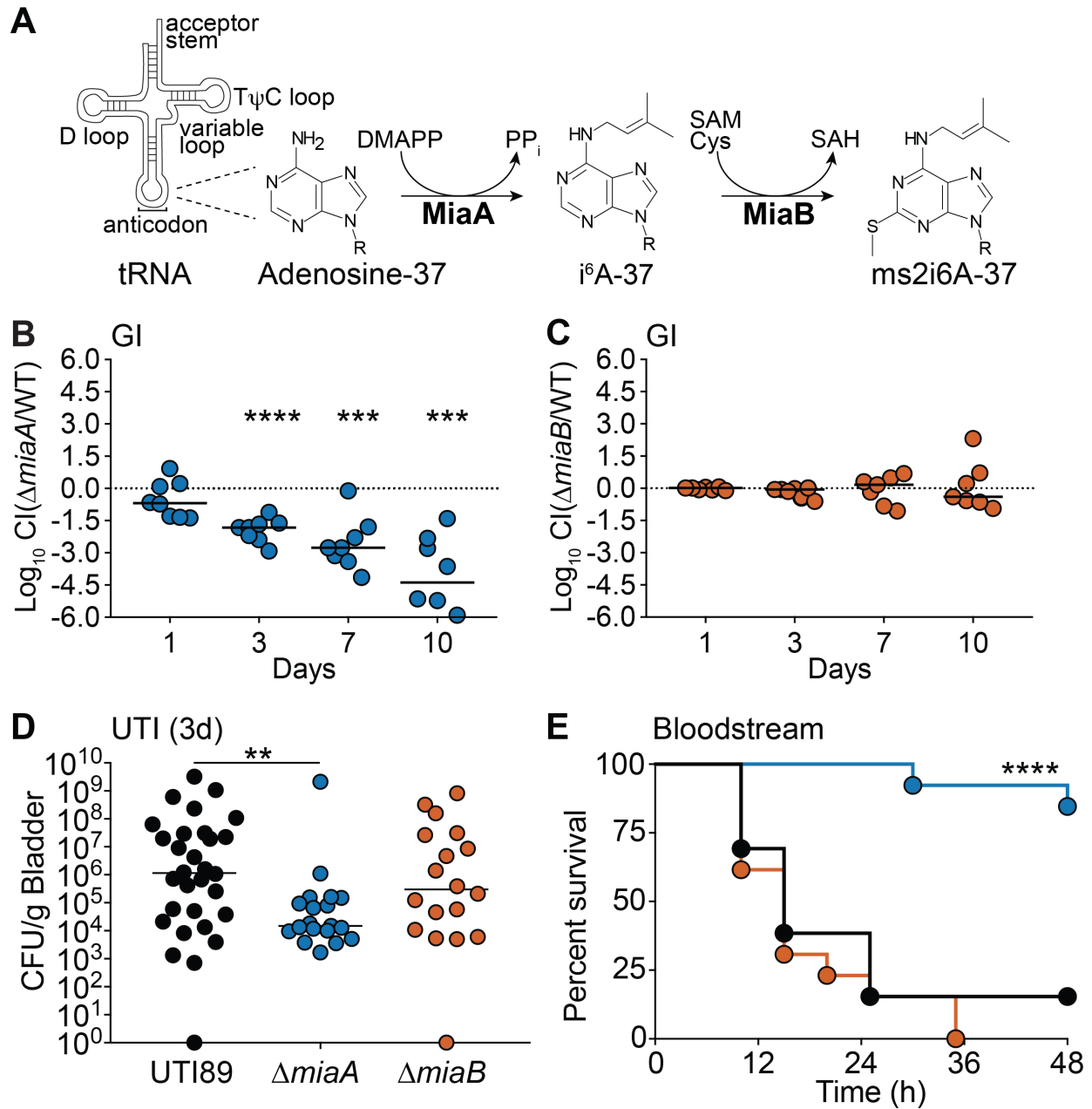
1220 **(A)** MiaA and MiaB act sequentially to modify tRNA molecules that recognize UNN
1221 codons; modified from [37]. DMAPP, dimethylallyl diphosphate; SAM, S-
1222 adenosylmethionine; SAH, S-adenosylhomocysteine; Cys, cysteine.

1223 **(B and C)** To assess gut colonization, adult BALB/c mice were inoculated via oral gavage
1224 with $\sim 10^9$ CFU of a 1:1 mixture of **(B)** UTI89 and UTI89 Δ *miaA* or **(C)** UTI89 and
1225 UTI89 Δ *miaB*. Fecal titers were determined at the indicated time points and used to
1226 calculate competitive indices (CI). ***, $P < 0.001$; ****, $P < 0.0001$ by one sample *t*-tests.
1227 $n = 7$ -8 mice from two independent experiments.

1228 **(D)** The bladders of adult female CBA/J mice were inoculated via transurethral
1229 catheterization with $\sim 10^7$ CFU of UTI89, UTI89 Δ *miaA*, or UTI89 Δ *miaB*. Mice were
1230 sacrificed 3 days later and bacterial titers within the bladders were determined by plating
1231 tissue homogenates. **, $P < 0.01$ by Mann Whitney U tests; $n \geq 19$ mice per group from
1232 at least three independent experiments. In B, C, and D, bars indicate median values; dots
1233 represent individual mice.

1234 **(E)** Kaplan Meier survival curves of C57Bl/6 mice inoculated via i.p. injections with $\sim 10^7$
1235 CFU of UTI89 (black line), UTI89 Δ *miaA* (blue), or UTI89 Δ *miaB* (orange). ****, $P < 0.0001$
1236 by Log-rank Mantel Cox test for UTI89 versus UTI89 Δ *miaA*; $n = 13$ mice per group from
1237 two independent experiments.

Figure 1



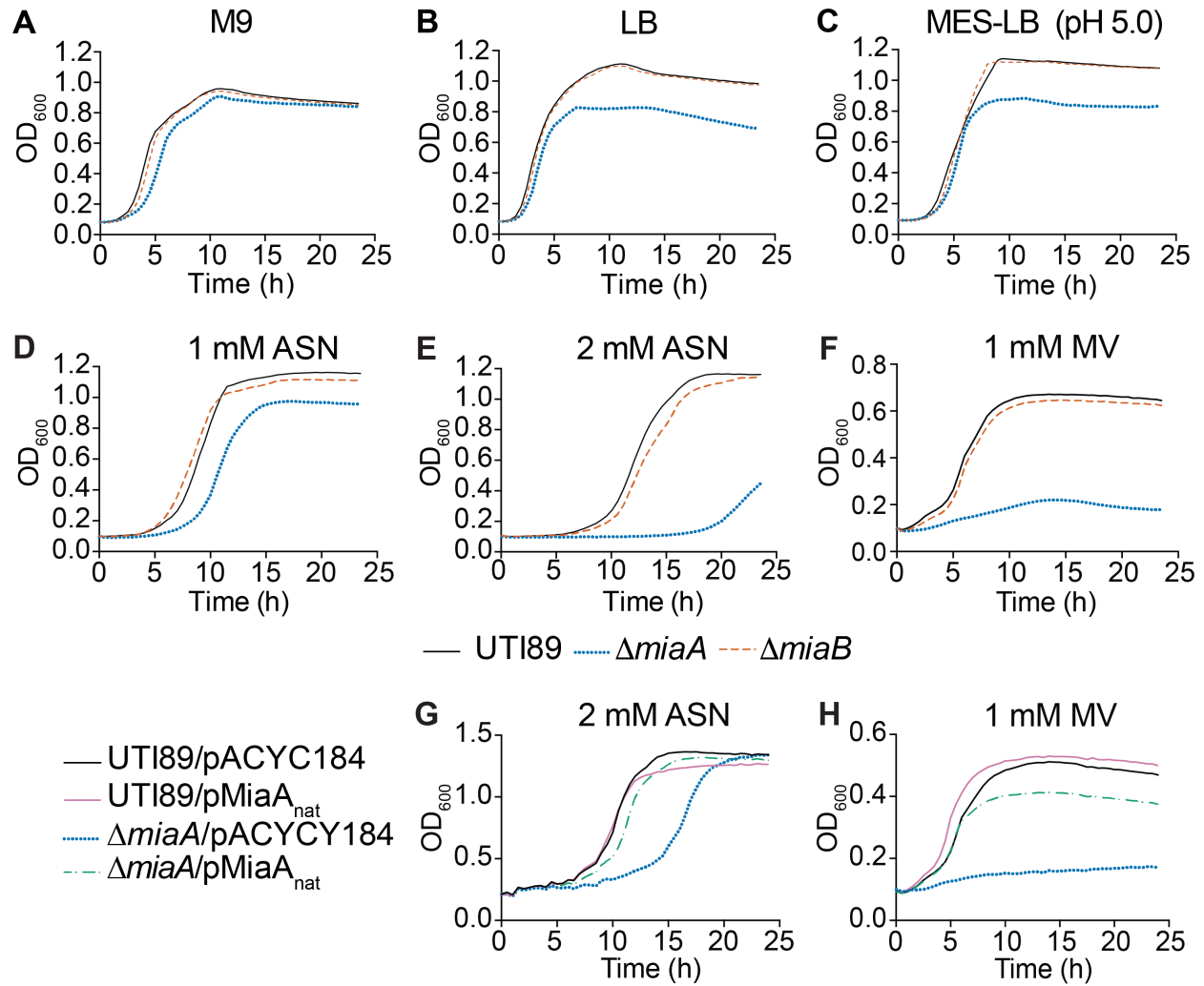
1238 **Figure 2. Deletion of *miaA* limits growth of UTI89 in rich medium and lowers**
1239 **resistance to oxidative and nitrosative stress.**

1240 **(A-F)** Graphs indicate mean growth of UTI89, UTI89 Δ *miaA*, and UTI89 Δ *miaB* in shaking
1241 cultures with modified M9 media, LB, MES-LB, MES-LB with 1 or 2 mM ASN, or LB with
1242 1 mM MV.

1243 **(G and H)** Curves show mean growth of UTI89 and UTI89 Δ *miaA* carrying pMiaA_{nat} (with
1244 *miaA* expressed from its native promoter) or the empty vector control pACYC184 in LB
1245 containing (G) 2 mM ASN or (H) 1 mM MV.

1246 Each curve shows the means of results from four replicates, and are representative of
1247 three independent experiments.

Figure 2



1248 **Figure 3. MiaA enhances the resistance of UTI89 to osmotic stress.**

1249 **(A)** Bacteria were grown to stationary phase in LB, pelleted, and resuspended in ddH₂O.

1250 The mean numbers (\pm SEM) of surviving bacteria recovered at the indicated time points

1251 are graphed as the percentage of the bacteria present immediately after resuspension in

1252 ddH₂O (time 0). *P*-values were determined by two-way ANOVA with the Geisser-

1253 Greenhouse correction; *n* = 3 independent assays each done in triplicate.

1254 **(B)** Bars indicate mean numbers of bacteria (\pm SD) that survived 2 hours in ddH₂O with

1255 0.1% glucose, calculated as a percent of the inoculum. *P* values were determined, relative

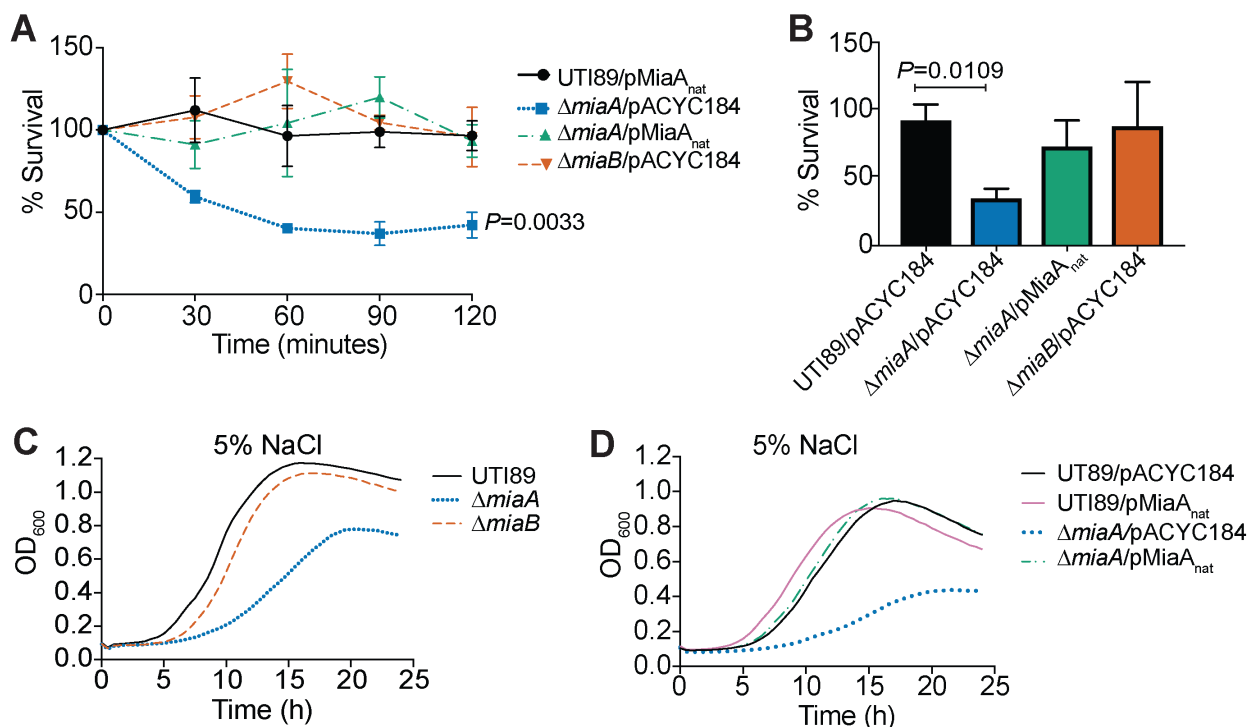
1256 to the control strain UTI89/pMiaA_{nat}, by unpaired *t*-tests with Welch's correction; *n* = 3

1257 independent assays.

1258 **(C and D)** Curves show growth of the indicated strains in LB plus 5% NaCl, as measured

1259 by OD₆₀₀. Data are representative of at least three independent experiments performed

1260 in quadruplicate.



1261

1262 **Figure 4. High salt stress downregulates MiaA translation and reduces ms²i⁶A**
1263 **levels.**

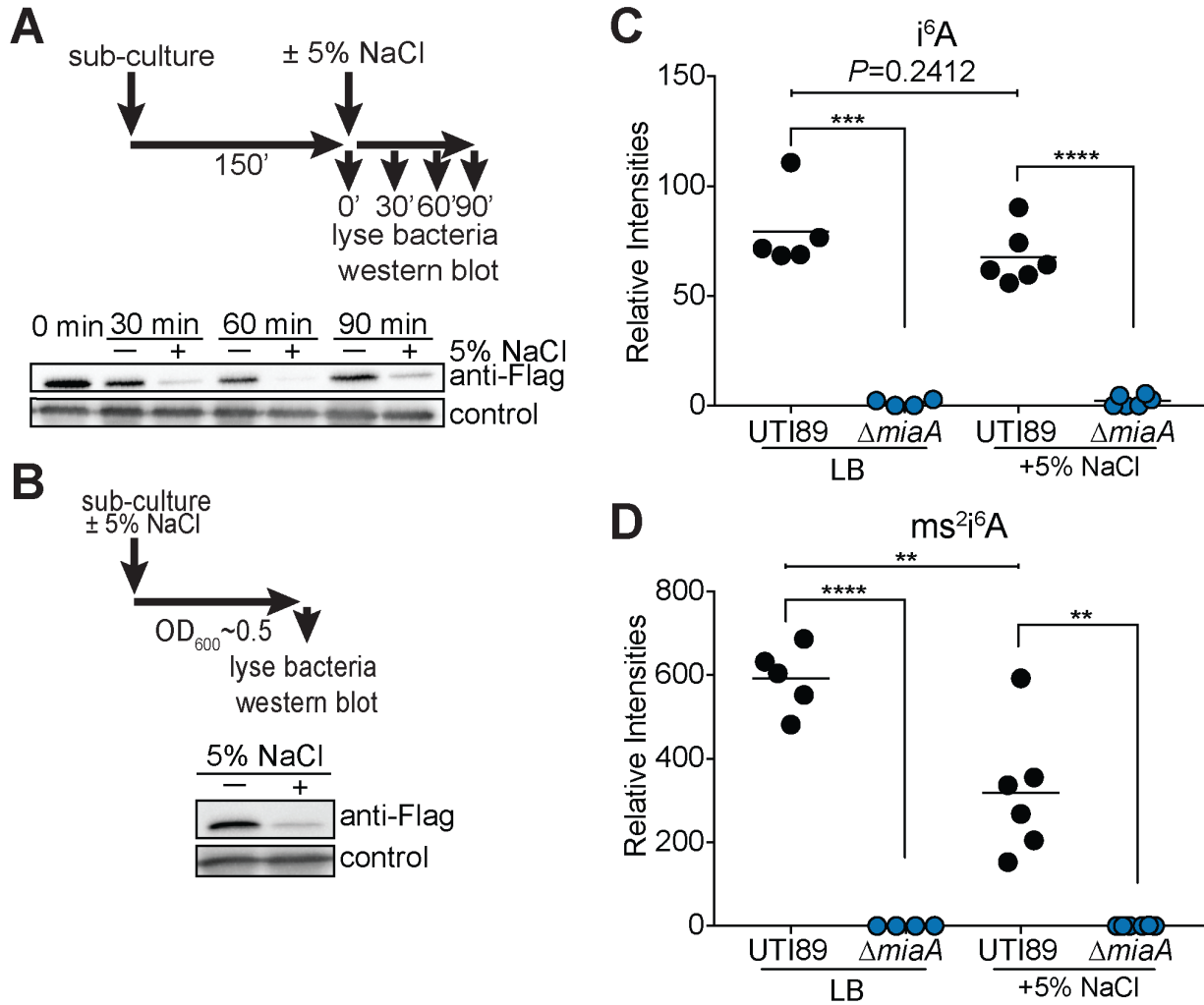
1264 **(A)** Top panel shows schematic of the experimental setup. UTI89/pMiaA-Flag_{nat} was
1265 diluted from overnight cultures into fresh LB and grown shaking for 2.5 hours at 37°C prior
1266 to resuspension in LB or LB + 5% NaCl. Incubations were continued for the indicated
1267 times before samples were collected and analyzed by western blots using anti-Flag and
1268 anti-*E. coli* (loading control) antibodies (bottom panel).

1269 **(B)** Top panel summarizes the experimental setup. Overnight cultures of UTI89/pMiaA-
1270 Flag_{nat} were diluted directly into fresh LB or LB + 5% NaCl and grown shaking to OD₆₀₀
1271 of 0.5 prior to processing for western blot analysis (bottom panel).

1272 **(C and D)** UTI89 from mid-logarithmic cultures in LB was resuspended in LB or LB + 5%
1273 NaCl and one hour later the levels of *miaA* and *miaB* transcripts were determined by RT-
1274 qPCR. Bars indicate mean values from 9 independent replicates, each with two technical
1275 replicates. *, $P < 0.05$; ***, $P < 0.001$ by Mann-Whitney U tests.

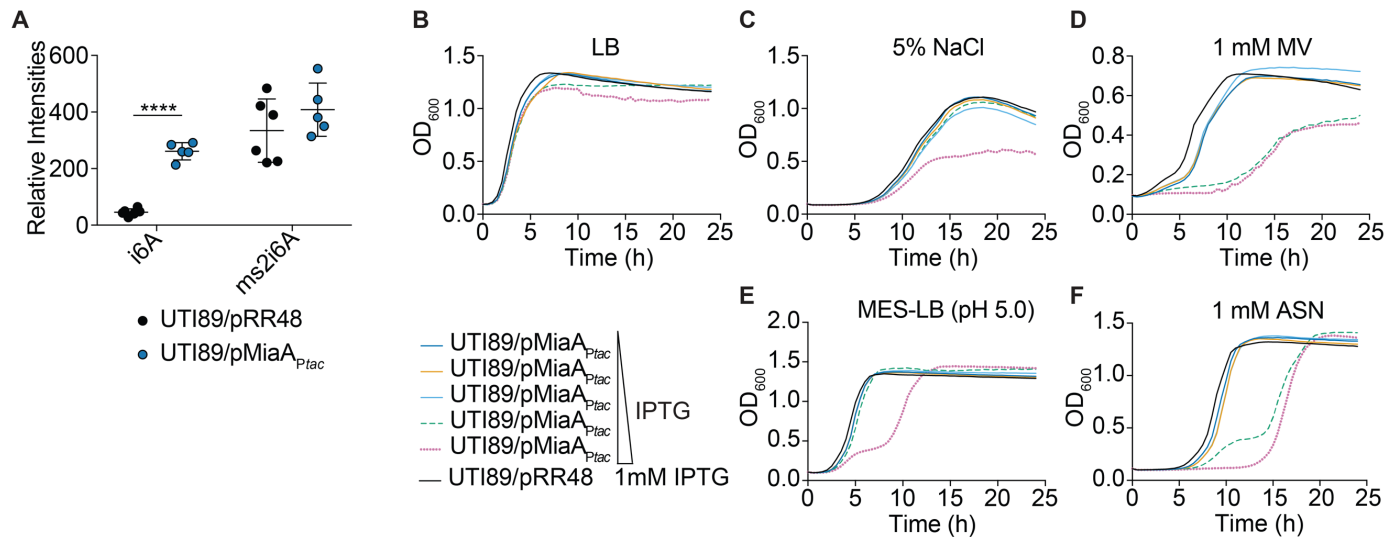
1276 **(E and F)** Graphs show relative levels of i⁶A and ms²i⁶A recovered from UTI89 and
1277 UTI89Δ*miaA* following growth to OD₆₀₀ of 0.5 in LB or LB + 5% NaCl, as determined by
1278 LC-MS. **, $P < 0.01$; ***, $P < 0.001$; ****, $P < 0.0001$ by unpaired *t* tests. Bars indicate
1279 median values from 4 to 6 independent replicates.

Figure 4



1280 **Figure 5. Overexpression of MiaA reduces ExPEC stress resistance.**

1281 **(A)** Relative levels of i^6A and ms^2i^6A in UTI89 carrying either $pMiaA_{Ptac}$ or the empty vector
1282 control pRR48 following growth to OD_{600} of 0.5 in LB with 1 mM IPTG, as quantified by
1283 LC-MS. ****, $P < 0.0001$ by unpaired t test; $n = 5$ to 6 independent replicates per group.
1284 **(B-F)** Curves depict growth of UTI89 carrying $pMiaA_{Ptac}$ or the empty vector control
1285 pRR48 in LB, LB + 5% NaCl, LB + 1mM MV, MES-LB, or MES-LB + 1 mM ASN. Cultures
1286 were grown shaking at 37°C with IPTG added in ten-fold increments from 0 to 1000 μ M,
1287 as indicated. Each curve depicts the means of results from a single experiment and is
1288 representative of at least three independent experiments carried out in quadruplicate.



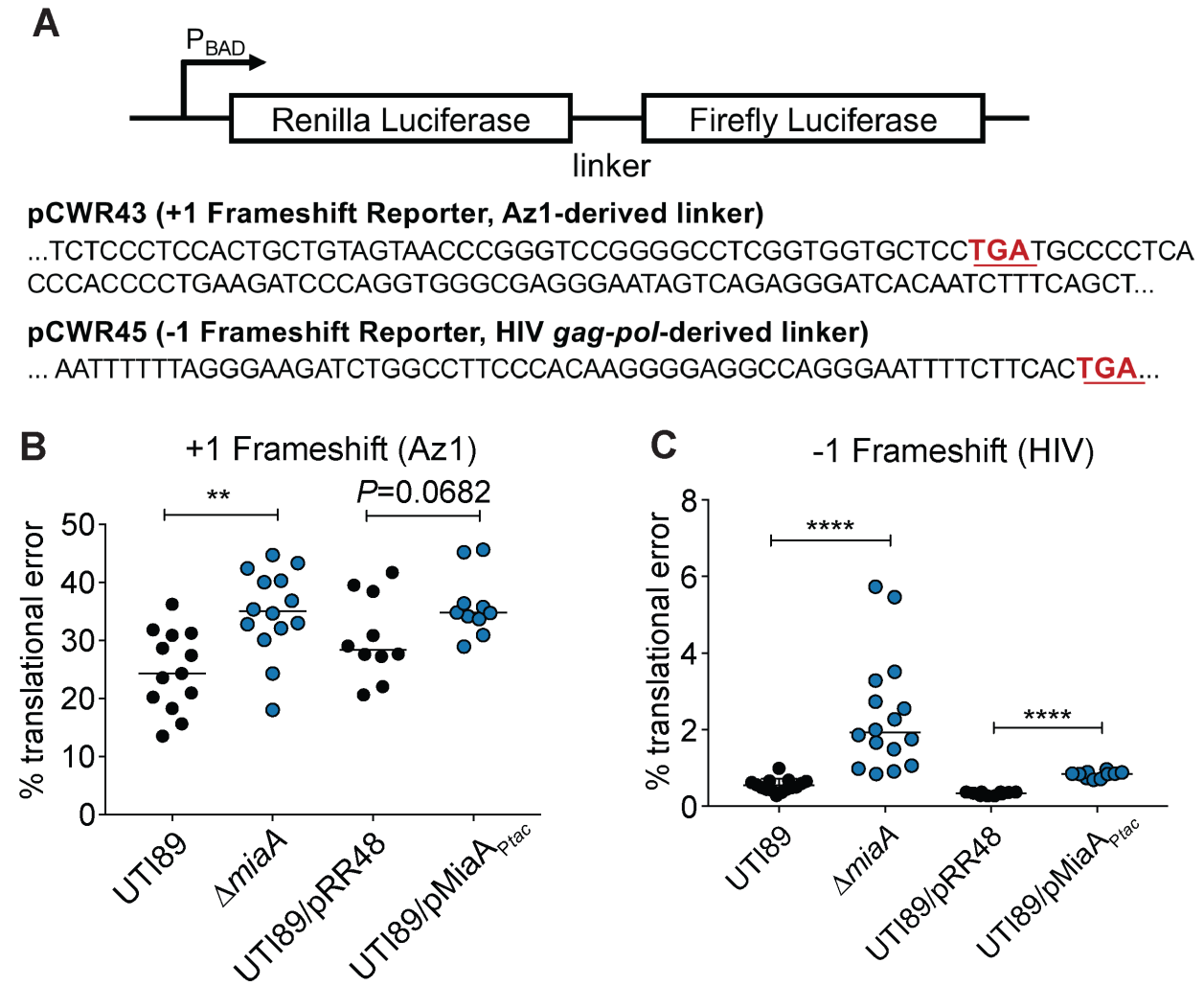
1289 **Figure 6. Changing levels of MiaA increase frameshifting.**

1290 **(A)** Diagram depicts the structures of the dual luciferase reporters, with specific intergenic
1291 linker sequences and premature stop codons (underlined red) indicated below. Each
1292 linker contains MiaA-sensitive UNN codons.

1293 **(B and C)** Graphs show results from +1 and -1 frameshifting assays with UTI89,
1294 UTI89 Δ *miaA*, UTI89/pRR48, or UTI89/pMiaA_{P_{tac}} carrying one of the dual luciferase
1295 reporter constructs. Bacteria were grown shaking at 37°C in LB, with 1 mM IPTG included
1296 for UTI89/pRR48 and UTI89/pMiaA_{P_{tac}}. After reaching an OD₆₀₀ of ~0.2, 0.2% arabinose
1297 was added to induce expression of the luciferases. At an OD₆₀₀ of 0.5, translational error
1298 rates were quantified by determining the ratio of firefly to renilla luciferase activities in
1299 bacteria carrying the +1 (Az1) and -1 (HIV) reporter constructs. Results were normalized
1300 using the ratio of firefly to renilla luciferase activity in bacteria carrying control plasmids in
1301 which the luciferases are in-frame. **, $P < 0.01$; ****, $P < 0.0001$ by two-tailed unpaired t
1302 tests; $n = 10-14$ independent replicates.

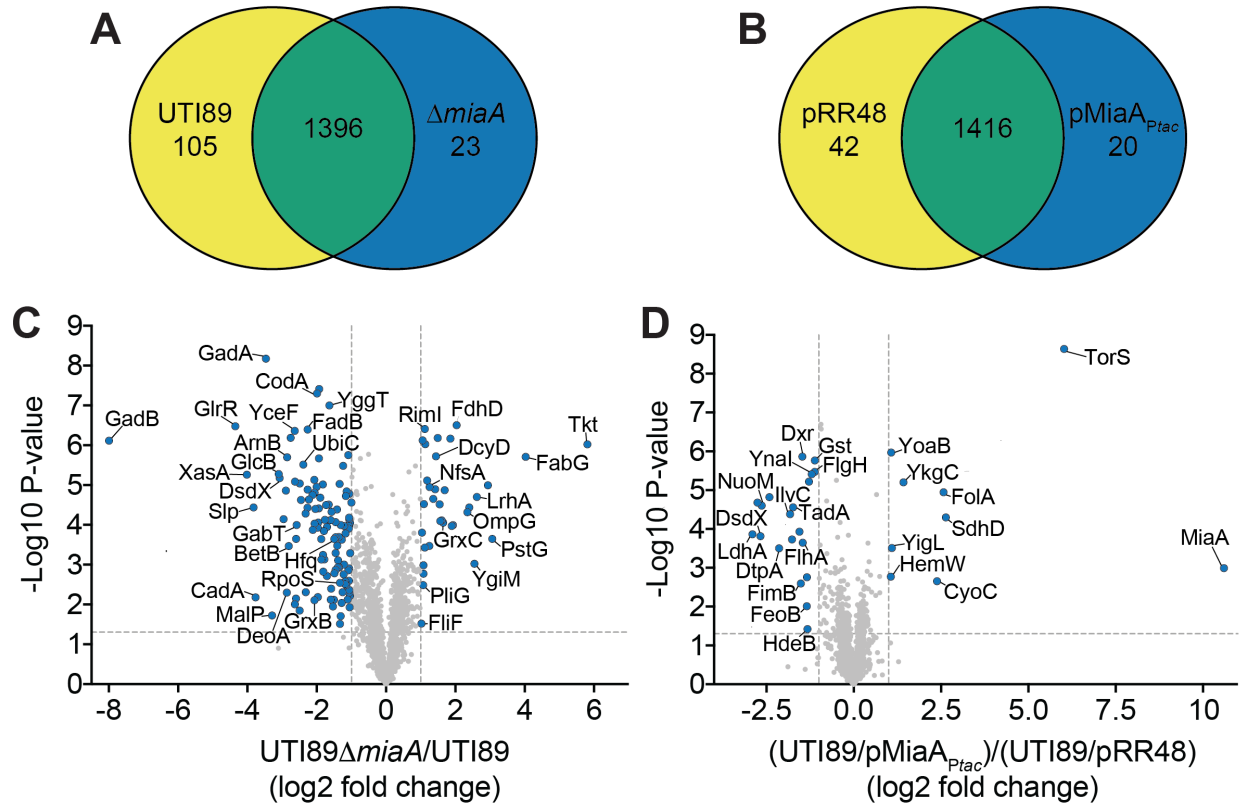
1303

Figure 6



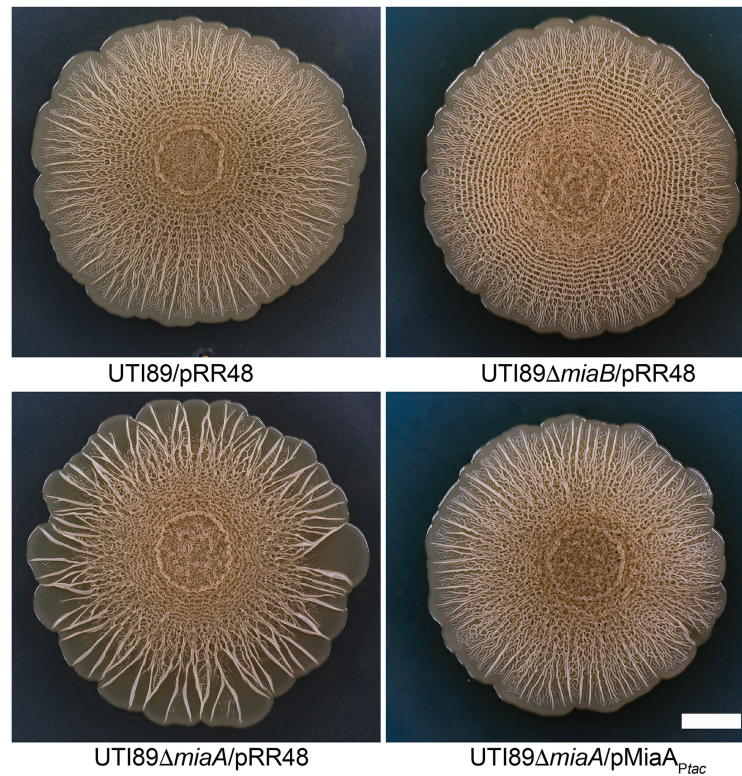
1304 **Figure 7. Altering MiaA levels changes the spectrum of expressed proteins.**
1305 **(A and B)** Venn diagrams indicate numbers of unique and shared proteins detected in
1306 wild-type UTI89 versus UTI89 Δ *miaA*, or in UTI89/pRR48 versus UTI89/pMiaA_{P_{ta}c},
1307 following growth to OD₆₀₀ of 0.5 in LB. IPTG (1 mM) was included in the UTI89/pRR48
1308 and UTI89/pMiaA_{P_{ta}c} cultures. Relative protein levels were determined by MudPIT.
1309 **(C and D)** Volcano plots show relative protein levels (Log₂-fold change) versus P-values
1310 (-Log₁₀). Proteins from UTI89 Δ *miaA* were quantified relative to the wild-type strain, while
1311 proteins levels from UTI89/pMiaA_{P_{ta}c} were assessed relative to UTI89/pRR48. The
1312 vertical dotted lines denote a 2-fold change, while the horizontal dotted lines indicate a P-
1313 value of 0.05. Blue dots indicate proteins that were significantly changed ($P < 0.05$) by at
1314 least 2-fold. P values were determined by Student's *t* tests; $n = 4$ independent replicates
1315 for each group.

Figure 7



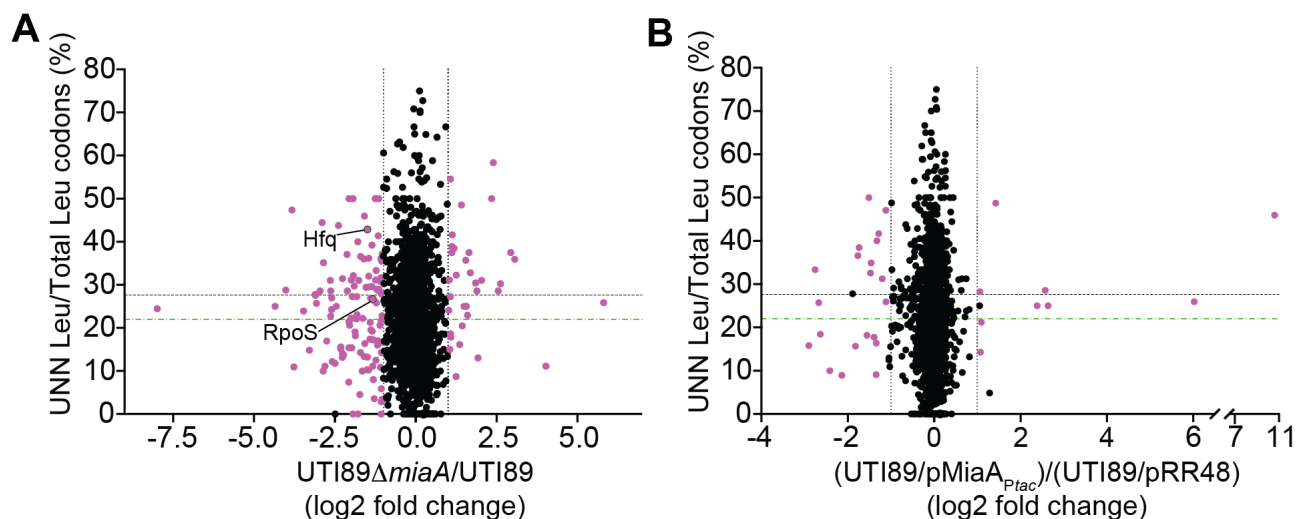
1316 **Figure 8. MiaA regulates ExPEC biofilm development.**

1317 Images show biofilms formed by wild-type UTI89 and its derivatives after 14 days of
1318 growth at room temperature on YESCA plates. Photos are representative of at least three
1319 independent replicates. Scale bar, 1 cm.



1320 **Figure 9. UNN-Leu codon usage ratios vary among MiaA-sensitive transcripts.**

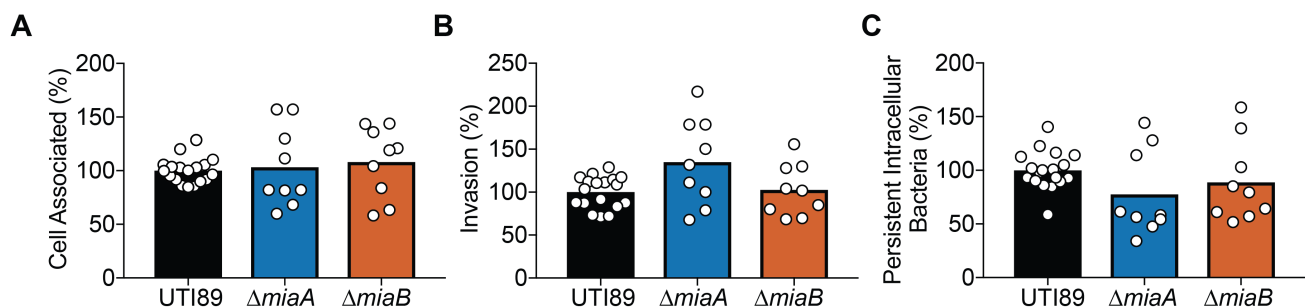
1321 **(A and B)** Plots show relative protein levels (Log₂-fold change) versus UNN-Leu codon
1322 usage ratios (UNN Leu/total Leu codons per open reading frame). Proteins in (A)
1323 UTI89Δ*miaA* were quantified by MudPIT relative to wild-type UTI89, while proteins levels
1324 in (B) UTI89/pMiaA_{P_{tac}} were calculated relative to UTI89/pRR48, as in Fig. 7. Purple dots
1325 denote proteins that were significantly changed ($P < 0.05$, by Student's *t* tests) by at least
1326 2-fold in UTI89Δ*miaA* or UTI89/pMiaA_{P_{tac}} relative to their controls. The vertical dotted lines
1327 are placed at the 2-fold change cutoffs. The green and black horizontal dashed lines
1328 indicate the average ratios of UNN-Leu codons relative to total Leu codons for all open
1329 reading frames encoded by the K-12 strain MG1655 and UTI89, respectively.



1330 **SUPPLEMENTAL INFORMATION**

1331 **Supplemental Figure S1: MiaA and MiaB do not affect the ability of ExPEC to bind,**
1332 **invade, or persist intracellularly within bladder epithelial cells.**

1333 Human bladder epithelial cells (5637 cells) were infected with UTI89, UTI89 Δ *miaA*, or
1334 UTI89 Δ *miaB* for 2 h, followed by a second 2-h incubation in the presence of the
1335 bactericidal, host cell-impermeable antibiotic gentamicin (100 μ g/ml). Graphs show (A)
1336 the levels of host cell-associated bacteria prior to the addition of gentamicin, (B) and the
1337 relative numbers of intracellular bacteria recovered after the 2-h incubation in media
1338 containing gentamicin. (C) Longer-term bacterial persistence within the bladder cells was
1339 assessed by continued incubation of infected host cells for an additional 12 h with
1340 gentamicin. For the longer persistence assays, a submaximal concentration of gentamicin
1341 (10 μ g/ml) was used to prevent extracellular growth of UPEC while limiting possible
1342 leaching of the antibiotic into the host cells. Data are expressed relative to wild-type
1343 UTI89, with bars indicating median values from 9 to 18 independent experiments
1344 performed in triplicate.

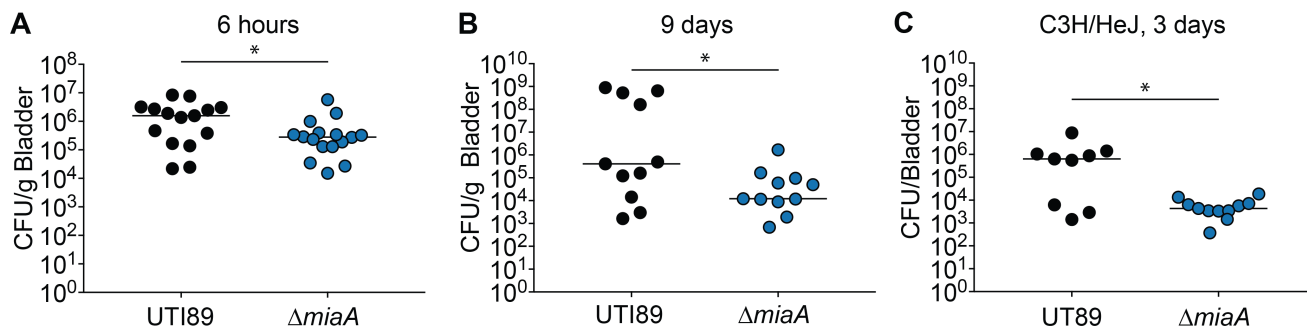


1345 **Supplemental Figure S2. MiaA promotes ExPEC colonization and persistence**
1346 **within the murine bladder.**

1347 **(A and B)** The bladders of adult female CBA/J mice were inoculated via transurethral
1348 injections with $\sim 10^7$ CFU of wild-type UTI89 or UTI89 $\Delta miaA$. Mice were sacrificed (A) 6
1349 hours or (B) 9 days later and bacterial titers within the bladders were determined by
1350 plating tissue homogenates.

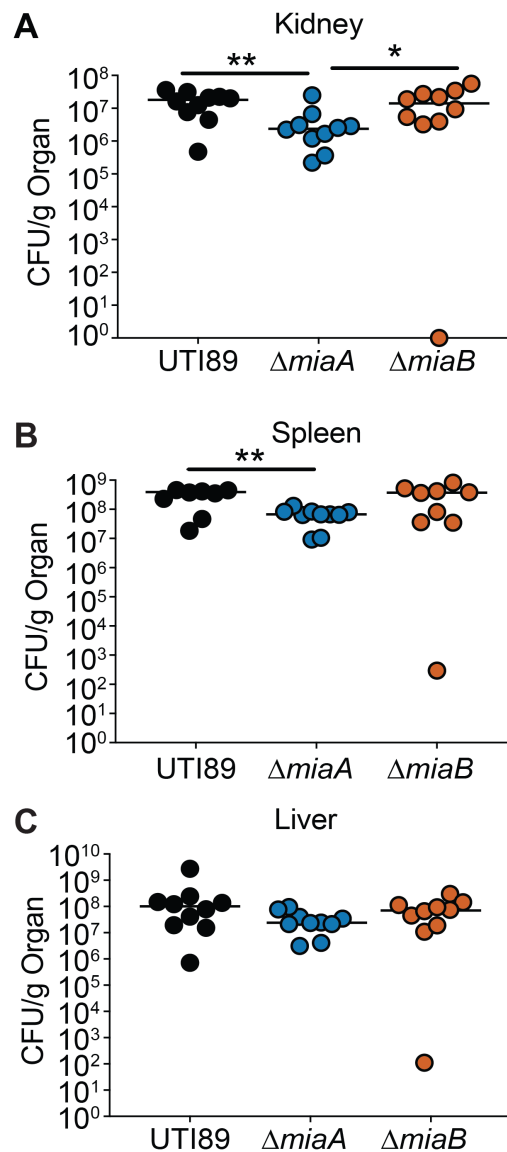
1351 **(C)** Graph shows bacterial titers recovered from the bladders of adult female C3H/HeJ
1352 mice 3 days after inoculation with UTI89 or UTI89 $\Delta miaA$.

1353 Bars in all graphs denote median values. *, $P < 0.05$ by Mann Whitney U tests; $n \geq 9$ mice
1354 per group.



1355 **Supplemental Figure S3. MiaA promotes ExPEC fitness in a mouse model of**
1356 **sepsis.**

1357 Adult female C57Bl/6 mice were inoculated via i.p. injections with 10^7 - 10^8 CFU of UTI89,
1358 UTI89 Δ *miaA*, or UTI89 Δ *miaB* and 6 hours later bacterial titers were present in the (A)
1359 kidneys, (B) spleen, and (C) liver were determined by plating tissue homogenates. *, $P <$
1360 0.05 and **, $P > 0.01$ by Mann Whitney U tests; $n = 10$ mice per group.

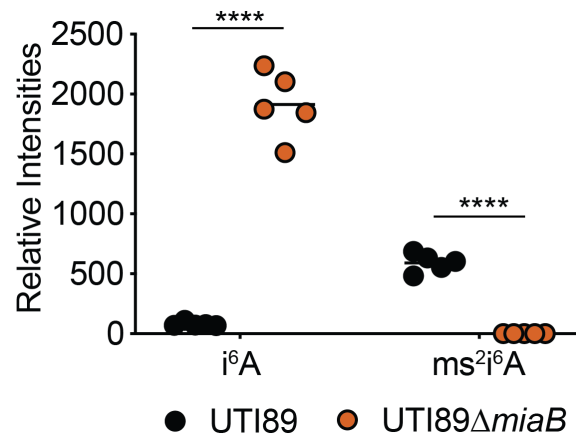


1361 **Supplemental Figure S4. The ms^2i^6A modification is missing in $UTI89\Delta miaB$.**

1362 RNA was collected from wild-type $UTI89$ and $UTI89\Delta miaB$ after reaching an OD_{600} of 0.5

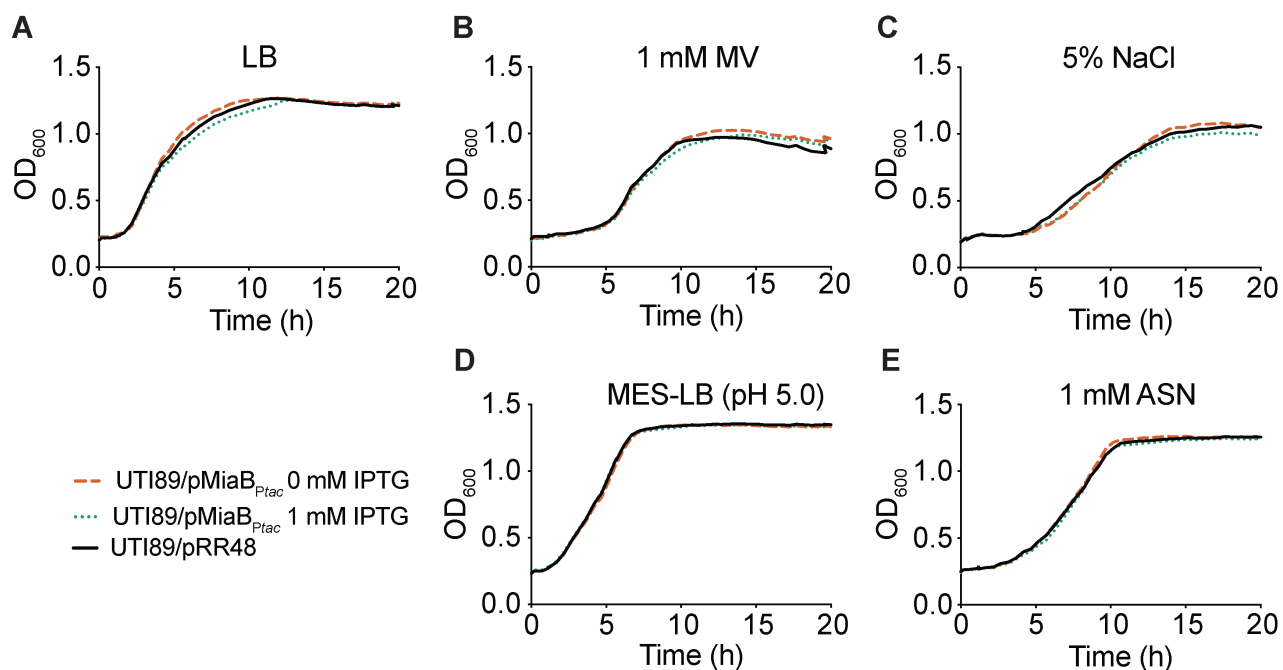
1363 in shaking LB cultures. Relative levels of i^6A and ms^2i^6A were determined by LC-MS. ****,

1364 $P < 0.0001$ as determined an unpaired t test; $n = 5$ independent replicates.



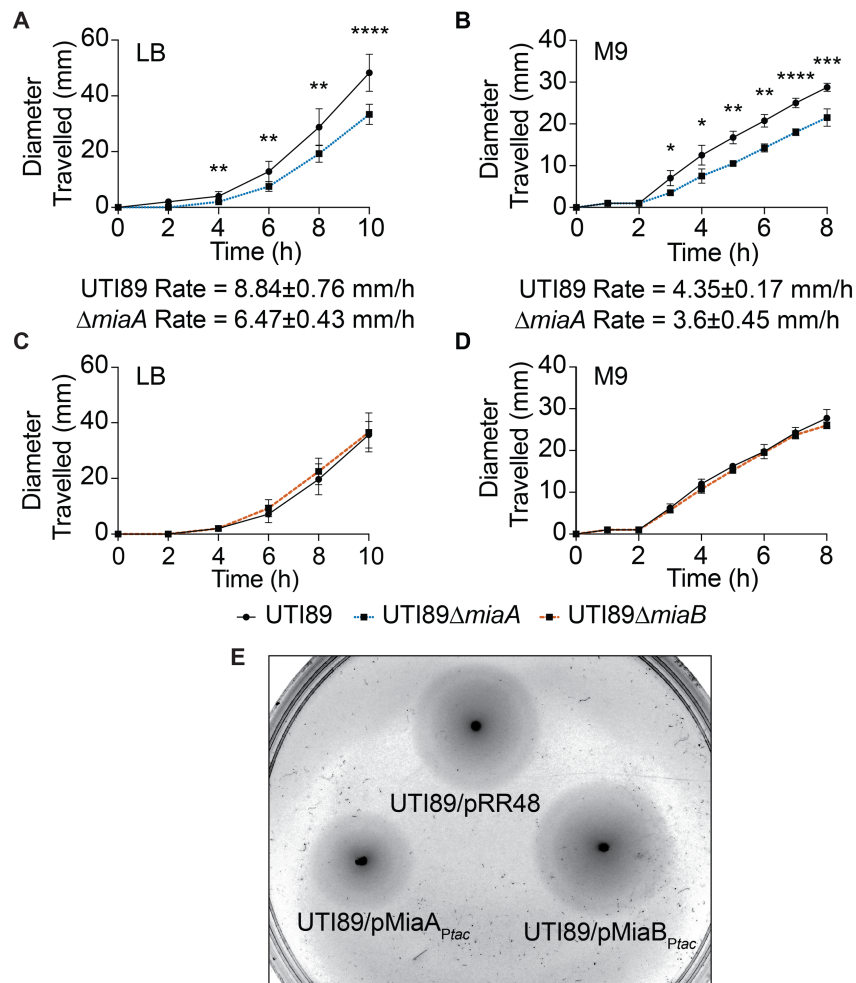
1365 **Supplemental Figure S5. Overproduction of MiaB does not affect growth of UTI89**
1366 **under stressful conditions.**

1367 Graphs show growth curves of UTI89 carrying pMiaB_{P_{tac}} or the control plasmid pRR48 in
1368 (A) LB, (B) 1 mM MV, (C) 5% NaCl, (D) MES-LB, and (E) 1 mM ASN. To overexpress
1369 MiaB, 1 mM IPTG was added to UTI89/pMiaB_{P_{tac}}. Data are representative of three or
1370 more independent experiments, each done in quadruplicate.



1371 **Supplemental Figure S6. MiaA modulates ExPEC motility.**

1372 (A - D) Graphs indicate the spread of UTI89 (black lines), UTI89 Δ *miaA* (dotted blue lines),
1373 and UTI89 Δ *miaB* (dashed red lines) on (A and C) LB and (B and D) M9 swim motility
1374 plates incubated at 37°C. Shown are mean values \pm SD from three independent
1375 experiments done in triplicate. Swim rates (\pm SD) for wild-type UTI89 and UTI89 Δ *miaA*
1376 on LB and M9 swim plates are indicated below the graphs in (A) and (B). *, $P < 0.05$; **,
1377 $P < 0.01$; ***, $P < 0.001$; ****, $P < 0.0001$ versus wild-type UTI89, as determined by
1378 unpaired *t* tests; $n \geq 4$ independent replicates. (E) Representative image showing the
1379 spread of UTI89/pRR48, UTI89/pMiaB_{P_{tac}}, and UTI89/pMiaA_{P_{tac}} 6 hours after inoculation
1380 onto an LB swim plate containing 1 mM IPTG and ampicillin.



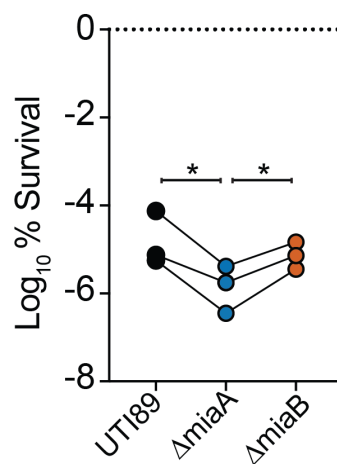
1381 **Supplemental Figure S7. UTI89 Δ *miaA* is has increased sensitivity to acid stress.**

1382 After reaching mid-logarithmic growth phase in LB, wild-type UTI89, UTI89 Δ *miaA*, and

1383 UTI89 Δ *miaB* were exposed to acidic stress (pH 3.0) for 30 min. Following washes in PBS,

1384 surviving bacteria were enumerated by dilution plating. Titers are normalized to input.

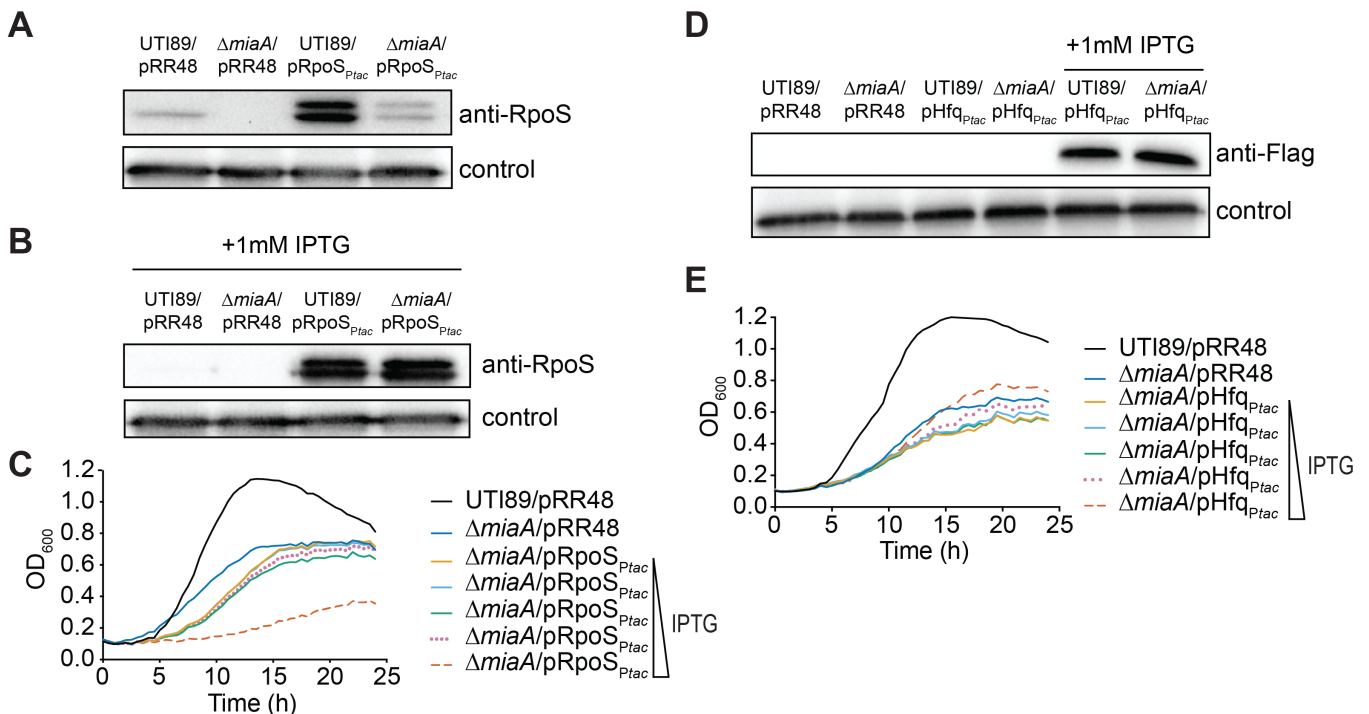
1385 Biological replicates are connected by lines. *, $P < 0.05$ by paired t tests.



1386 **Supplemental Figure S8. Expression of RpoS or Hfq does not rescue growth of**
 1387 **UTI89 Δ *miaA* in the presence of high salt stress.**

1388 **(A - C)** Western blots of RpoS and Flag-tagged Hfq in UTI89 and UTI89 Δ *miaA* carrying
 1389 pRpoS_{P_{tac}}, pHfq_{P_{tac}}, or the empty vector pRR48 following growth to stationary phase in
 1390 LB or LB with 1 mM IPTG, as indicated. As a loading control, blots were also probed with
 1391 anti-*E. coli* antibody. A shorter exposure was used for the blot shown in (B), making the
 1392 RpoS band from UTI89/pRR48 notably lighter than the one shown in (A). Blots are
 1393 representative of three independent experiments.

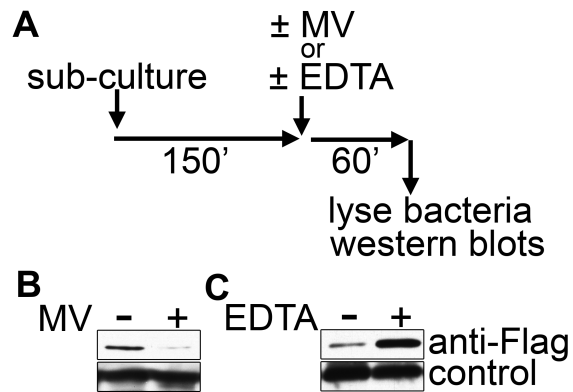
1394 **(D and E)** Curves show growth of the UTI89 and UTI89 Δ *miaA* with the empty vector
 1395 pRR48 or plasmids for IPTG-inducible expression of RpoS or Flag-tagged Hfq in LB + 5%
 1396 NaCl. Cultures were grown shaking at 37°C with IPTG added in ten-fold increments from
 1397 0 to 1000 μ M, as indicated. Each growth curve shows the means of results from a single
 1398 experiment and is representative of at least three independent experiments performed in
 1399 quadruplicate.



1400 **Supplemental Figure S9. Methyl viologen and EDTA alter MiaA levels.**

1401 (A) Top panel shows schematic of the experimental setup. UTI89/pMiaA-Flag_{nat} was
1402 diluted from overnight cultures into fresh LB and grown shaking for 2.5 hours at 37°C prior
1403 to resuspension in LB, LB + 5% NaCl, or LB + 1 mM EDTA. Incubations were continued
1404 for another hour before samples were collected and analyzed by western blots.

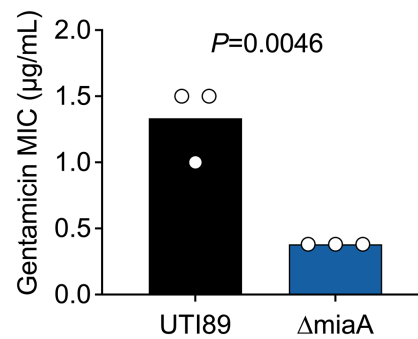
1405 (B and C) Blots were probed using anti-Flag (MiaA-Flag) and anti-*E. coli* (loading control,
1406 bottom) antibodies.



1407 **Supplemental Figure S10. UTI89 Δ *miaA* is more sensitive to gentamicin than the**
1408 **wildtype UTI89.**

1409 Bars in graph indicate mean MIC values (\pm SD) determined from three independent
1410 Etests. *P*-value was determined by an unpaired Student's *t* test.

1411



Supplemental Table S1. Bacterial strains and plasmids

Strain or Plasmid	Description	Source or Reference
Strains		
UTI89	UPEC reference strain, cystitis isolate	[52, 108]
UTI89::Kan ^R	UTI89 with a Kan ^R resistance cassette inserted at the <i>attTn7</i> site	This study
UTI89Δ <i>miaA</i>	UTI89 <i>miaA</i> ::Cam ^R	This study
UTI89Δ <i>miaB</i>	UTI89 <i>miaB</i> ::Cam ^R	This study
Plasmids		
pACYC184	Low-copy number plasmid; Tet ^R , Cam ^R	New England Biolabs
pBAD18	Arabinose-inducible bacterial expression plasmid; Amp ^R	[109]
pBAD33	Arabinose-inducible bacterial expression plasmid; Cam ^R	[109]
pKD3	Carries FRT-flanked Cam ^R cassette; template for use in lambda-Red-mediated recombination	[48]
pKD4	Carries FRT-flanked Kan ^R cassette; template for use in lambda-Red-mediated recombination	[48]
pKM208	IPTG-inducible lambda Red recombinase expression plasmid; Amp ^R	[49]
pRR48	Contains IPTG-inducible P _{tac} promoter upstream of the MCS; Amp ^R	[110]
pHfq _{P_{tac}}	<i>hfq</i> from UTI89 cloned with c-terminal 6xHis and FLAG tags into PstI, HindIII sites of pRR48; Amp ^R	This Study
pRpoS _{P_{tac}}	<i>RpoS</i> cloned from UTI89 into PstI, HindIII sites of pRR48; Amp ^R	[62]
pMiaA _{P_{tac}}	<i>miaA</i> cloned from UTI89 into PstI, KpnI sites of pRR48; Amp ^R	This study
pMiaB _{P_{tac}}	<i>miaB</i> cloned from UTI89 into PstI, KpnI sites of pRR48; Amp ^R	This study
pMiaA _{nat}	<i>miaA</i> plus 200 bp of flanking sequences cloned from UTI89 into the EcoR1 site of pACYC184; Tet ^R	This study
pMiaA-Flag _{nat}	pACYC184-derived plasmid encoding MiaA with N-terminal Flag tag plus linker under control of native <i>miaA</i> promoter; Tet ^R	This study

p2Luc-HIV	Eukaryotic reporter construct with the HIV <i>gag-pol</i> frameshift region inserted between the renilla and firefly luciferase genes. The HIV linker sequence contains a 2-nucleotide insertion resulting in a stop codon located 6 codons after the start of firefly luciferase gene. The firefly gene is in a -1 frame relative to the upstream renilla gene; Amp ^R	Derived from [76]
p2Luc-HIV-IF	Control for p2Luc-HIV. The HIV <i>gag-pol</i> linker was altered to keep the renilla and firefly luciferases in-frame; Amp ^R .	Derived from [76]
p2Lucaz1	Eukaryotic reporter construct with the Az1 frameshift region inserted between the renilla and firefly luciferase genes. The Az1 linker sequence contains a stop codon positioned in-frame so that a +1 frameshift must occur for read-through expression of firefly luciferase; Amp ^R	[75]
p2Lucaz1-IF	Control for p2Lucaz1. The Az linker was altered to keep the renilla and firefly luciferases in-frame; Amp ^R	[75]
pCWR42-CamR	Dual luciferase reporter with in-frame Az1 linker cloned from p2Lucaz1-IF into pBAD33. Has a Shine-Dalgarno sequence and is under control of the arabinose-inducible P _{BAD} promoter. Control for pCWR43-CamR; Cam ^R	This study
pCWR42-AmpR	Dual luciferase reporter with in-frame Az1 linker cloned from p2Lucaz1-IF into pBAD18. Has a Shine-Dalgarno sequence and is under control of the arabinose-inducible P _{BAD} promoter. Control for pCWR43-AmpR; Amp ^R	This study
pCWR43-CamR	Dual luciferase reporter with Az1 linker cloned from p2Lucaz1 into pBAD33. Has a Shine-Dalgarno sequence and is under control of the arabinose-inducible P _{BAD} promoter; Cam ^R	This study
pCWR43-AmpR	Dual luciferase reporter with Az1 linker cloned from p2Lucaz1 into pBAD18. Has a Shine-Dalgarno sequence and is under control of the arabinose-inducible P _{BAD} promoter; Amp ^R	This study
pCWR44-CamR	Dual luciferase reporter with in-frame HIV linker cloned from p2Luc-HIV-IF into pBAD33. Has a Shine-Dalgarno sequence and is under control of the arabinose-inducible P _{BAD} promoter. Control for pCWR45-Cam; Cam ^R	This study

pCWR44-AmpR	Dual luciferase reporter with in-frame HIV linker cloned from p2Luc-HIV-IF into pBAD18. Has a Shine-Dalgarno sequence and is under control of the arabinose-inducible P _{BAD} promoter. Control for pCWR45-Amp; Amp ^R	This study
pCWR45-CamR	Dual luciferase reporter with HIV linker cloned from p2Luc-HIV into pBAD33. Has a Shine-Dalgarno sequence and is under control of the arabinose-inducible P _{BAD} promoter; Cam ^R	This study
pCWR45-AmpR	Dual luciferase reporter with HIV linker cloned from p2Luc-HIV into pBAD18. Has a Shine-Dalgarno sequence and is under control of the arabinose-inducible P _{BAD} promoter; Cam ^R	This study

Supplemental Table S2. Primers used in this study

Primer Name ^a	Sequence (5'-3') ^b
<i>Cloning primers</i>	
MiaA-pRR48-F	CGCGCTGCAGATGAGTGATATCAGTAAGGCG
MiaA-pRR48-R	CGGCGGTACCTCAGCCTGCGATAGCACCAAC
MiaB-pRR48-F	CGCGCTGCAGATGACCAAAA AACTCCATAT TAAAACC
MiaB-pRR48-R	CGGCGGTACCGAATTACGGCTGATAATAAC
MiaA-Flag-pACYC184-F	CGGCGAATTCGGCTAAAAGTTTCTGGCGAAGAAAAATCGG
MiaA-Flag-pACYC184-R	CGCGGAATTCCTATCCCTTATCGTCGTCATCCTTGTAGTCTGGTCCTCCTCCTCC GCCTGCGATAGCACCAACAAC
MiaA-pACYC184-F	CGCGGAATTCGCCCTTAGCCATTCTCTCTTTTTCCTTATATG
MiaA-pACYC184-R	CGGCGAATTCCCAGTCCGATGCGCAGCATGTGACCATC
Hfq-pRR48-PstI	CATACCTGCAGATGGCTAAGGGGCAATCTT
Hfq-CFLAG-his-HindII	CATACAAGCTTCTAGTGGTGGTGGTGGTGGTGTCCCTTATCGTCGTCATCCTTGTAGTCTCC TTCGGTTTCTTCGCTGTCCT
p2Luc-F	GCCGGGGTACCAGGAGGTCAGTCAGATGACTTCGAAAGTTATGATCCAG
p2Luc-R	GCCGGAAGCTTTTACAATTTGGACTTTCCGCCC
<i>Knockout, insertion, and confirmation primers</i>	
attTn7KanR-KI-F	TCTGGCGTAGCCTGGGAGTTATTGCCGGATGCGATGCTGGTGTGTAGGCTGGAGCTGCTTCG
attTn7KanR-KI-R	TCACGTAAAAAACGTCTAATCCGTAGACCGGATAAGAGGCCATATGAATATCCTCCTTAG
MiaA-KO-F	CGATAAAAGCCCTGAAAGATGAGTGATATCAGTAAGGCTGTGTAGGCTGGAGCTGCTTCG
MiaA-KO-R	CGTCTCCTGACGTTTGCGTCAGTTCGGTTAAAGTTTTACCCATATGAATATCCTCCTTAG
MiaA-KO-Conf-F	GCCGCCGGGTGGTCTGTGTTAC
MiaA-KO-Conf-R	CAGCCTGCGATAGCACCAAC
MiaB-KO-F	CCTGCATTCTGGCTACTATTTTCGCAAGAGCAAGTCGTGTGTAGGCTGGAGCTGCTTCG
MiaB-KO-R	CGGCGGGCCTGAGAATTACGGCTGATAATAACCCACGCCATATGAATATCCTCCTTAG
MiaB-KO-Conf-F	GCCGACCATTCTCCGCCGAC
MiaB-KO-Conf-R	CATTGTCTGCTGGCTCCAGG
<i>RT-qPCR primers</i>	
miaA-F	TACGGACTTGCCTTCCATTC
miaA-R	GCGCAAACACCTCGATAAAC
miaB-F	GTAGAAGGTACATCGCGTAAG
miaB-R	TCGGGTAGACGTCGGTAAT
rpoD-F	TTCGTACGCAAGAACGTCTG
rpoD-R	AGGTATCGCTGGTTTCGTTG

^a F, forward primer; R, reverse primer; KO, knockout primer; KI, knock-in primer; Conf, confirmation primer. ^b Added restriction sites in cloning primers underlined.